Dissection of the host-pathogen interaction in human tuberculosis using a bioengineered 3-dimensional model

Liku B Tezera[1], Magdalena K Bielecka[1], Andrew Chancellor[1], Michaela T Reichmann[1], Basim Al Shammari[2], Patience Brace[1], Alex Batty[1], Annie Tocheva[1], Sanjay Jogai[1], Ben G Marshall[1], Marc Tebruegge[1], Suwan N Jayasinghe[3], Salah Mansour[1,4], Paul Elkington[1,4]

[1]NIHR Respiratory Biomedical Research Unit, Clinical and Experimental Sciences Academic Unit, Faculty of Medicine, University of Southampton, UK. [2]King Abdullah International Medical Research Center/King Saud bin Abdulaziz University for Health Sciences, Department of Infectious Diseases, MNGHA, Riyadh, Saudi Arabia. [3]BioPhysics Group, UCL Institute of Biomedical Engineering, UCL Centre for Stem Cells and Regenerative Medicine and UCL Department of Mechanical Engineering, University College London, UK. [4]Institute for Life Sciences, University of Southampton, UK.

*** Address for correspondence:**

Professor Paul T Elkington

Clinical and Experimental Sciences

University of Southampton, Southampton SO16 1YD

Tel 00 44 23 8079 6671

E-mail: p.elkington@soton.ac.uk

Running title: Bioengineering human tuberculosis

Abstract

Cell biology differs between traditional cell culture and 3-dimensional (3-D) systems, and is modulated by the extracellular matrix. Experimentation in 3-D presents challenges, especially with virulent pathogens. *Mycobacterium tuberculosis* (Mtb) kills more humans than any other infection and is characterised by a spatially organised immune response and extracellular matrix remodelling. We developed a 3-D system incorporating virulent mycobacteria, primary human blood mononuclear cells and collagen–alginate matrix to dissect the host-pathogen interaction. Infection in 3-D led to greater cellular survival and permitted longitudinal analysis over 21 days. Key features of human tuberculosis develop, and extracellular matrix integrity favours the host over the pathogen. We optimised multiparameter readouts to study emerging therapeutic interventions: cytokine supplementation, host-directed therapy and immunoaugmentation. Each intervention modulates the host-pathogen interaction, but has both beneficial and harmful effects. This methodology has wide applicability to investigate infectious, inflammatory and neoplastic diseases and develop novel drug regimes and vaccination approaches.

Introduction

An emerging paradigm in biology is that events in traditional 2-dimensional cell culture often differ from those in 3-dimensional (3-D) culture (1, 2). Furthermore, the extracellular matrix regulates cell biology (3-5) and infection biology differs between 2-D and 3-D systems (6, 7). Human disease occurs in 3-D and in the context of extracellular matrix. Consequently, conclusions drawn from 2-dimensional cell culture systems may not fully reflect events *in vivo* (3). This presents a challenge to progress from standard culture systems, where cells are grown in 2-D on plastic, to more advanced systems that more faithfully replicate events in man (3). These technical difficulties are particularly marked in studying infectious diseases, where experiments must have additional levels of containment to prevent the release of pathogens (7).

Mycobacterium tuberculosis (Mtb) is a pathogen of global significance that continues to kill 1.5 million people per year (8, 9). Unfortunately, despite major investment in research, recent clinical trials and vaccine studies to reduce the global burden of tuberculosis (TB) have been unsuccessful (10-12), indicating that the model systems that informed these studies require further refinement. In TB, the host-pathogen interaction is highly complex, with the immune response concurrently necessary for containment of infection but paradoxically also driving immunopathology that leads to lung destruction and transmission (13, 14). The mouse is the principal model system to study TB, but inflammatory conditions in the mouse differ from man (15), and lung pathology is different in murine Mtb infection (16). Mtb is an obligate human pathogen and has a very prolonged interaction with host cells, surviving within professional phagocytes (13). Therefore, long term human culture experiments are required to investigate pathogenesis. A specific advantage of 3-D cell culture incorporating extracellular matrix is that cellular survival is greatly prolonged (17, 18). Furthermore, inflammatory signalling in TB granulomas is spatially organised (19), with specific microenvironments (20), and the extracellular matrix regulates cell survival in TB (21), indicating that an optimal system to study human disease will need to be 3-D with extracellular matrix.

We hypothesised that to fully understand the host-pathogen interaction in TB, a 3-D cell culture system that incorporates primary human cells, extracellular matrix, fully virulent Mtb, and multiparameter longitudinal readouts is required. Whilst human cellular models of human granuloma formation have been developed, none have all these characteristics (22-25). We addressed the technical challenges of performing these experiments at biosafety containment level 3 by adopting a bioengineering approach (26). We developed a model system that permits interrogation of the host-pathogen interaction in 3-D in the context of extracellular matrix. We demonstrate that cardinal features of human disease develop and that the host immune response is significantly different when cells are adherent to collagen, favouring the host relative to the pathogen. We investigate emerging therapeutic approaches in the system, and demonstrate that each intervention has both beneficial and likely harmful effects. The model permits the concurrent analysis of multiple outcomes and therefore can be used to develop optimal approaches to address the TB pandemic, and can be applied to diverse infectious, inflammatory and neoplastic diseases.

Results

Key features of human tuberculosis develop in the bio-electrospray model

To address the challenges of studying infection of primary human cells with a virulent pathogen within a 3-D extracellular matrix, we optimised the bio-electrospray parameters for stable microsphere generation. PBMCs were isolated from healthy donors, counted and then infected with Mtb that had been cultured in Middlebrook 7H9 broth at a multiplicity of infection of 0.1. After overnight infection, cells were detached, resuspended, and pelleted by centrifugation, and then re-suspended in alginate or alginate-collagen matrix before bioelectrospraying into microspheres using a Nisco Cell Encapsulator (Supplementary video 1 Figure 1 - figure supplement 1 and supplement 2). Characterisation of different alginates indicated that ultrapure medium viscosity guluronate (MVG)-dominant alginate had optimal biophysical properties for electrospraying and minimal immunogenicity (Figure 1 - figure supplement 3).

Immediately after generation, cells are evenly distributed within microspheres and by day 7 cellular aggregates start to form (Figure 1A and 1B). Quantitation demonstrated significantly more aggregates in infected microspheres than unifected microspheres (Figure 1C). One day after infection, a quarter of monocytes had phagocytosed Mtb, analyzed by flow cytometric analysis of cells infected with GFP-expressing Mtb (Figure 1D). After 14 days of incubation, large cellular aggregates are observed (Figure 1E). Survival of Mtb-infeced cells in 3-D collagen-alginate microspheres was much greater than in 2-D culture, as analyzed by LDH release (Figure 1F) and cellular cytotoxicity assays (Figure 1G). An advantage of the model is that cells can be released from the microsphere by decapsulation by divalent cation chelation with EDTA and sodium citrate in HBSS for 10 minutes, which causes dissolution of the spheres and releases cells for downstream assays. Decapsulation did not significantly affect cell viability, with over 90% cell viability after decapsulation (Figure 1 - figure supplement 4). Monocytes mature into macrophages in infected microspheres, with greater expression of CD68 (Figure 1H). Within the aggregates, multinucleate

giant cells typical of human TB develop, stained for CD68 by immunohistochemistry (Figure 1I). These multinucleate giant cells are similar to those that occur in human patients with pulmonary TB (Figure 1J). T cell differentiation occurs within microspheres, with a progressive increase in the proportion of CD4+ T cells, while the percentage of CD8+ T cells declines (Figure 1 - figure supplement 5). T cell proliferation does not differ between Mtb-infected and uninfected microspheres.

Next, we measured Mtb growth within microspheres longitudinally by infecting cells with luminescent Mtb expressing the Lux operon, which is genetically modified to constantly luminesce (27). Mtb in microspheres without human cells grows relatively slowly, whereas in the presence of PBMCs Mtb proliferates over 24 days, reaching the same luminescence as growth in 7H9 broth (Figure 2A). Proteases implicated in TB pathogenesis are upregulated, with MMP-1 gene expression increased within spheres 4 days post infection (Figure 2B) and MMP-9 accumulation in media surrounding the spheres peaking at day 7 (Figure 2C). This protease activity has a functional effect, causing increased degradation of fluorescently labelled collagen within microspheres (Figure 2D). Mtb infection also upregulated gene expression of IFN-γ (Figure 2E) and drives secretion of multiple pro-inflammatory cytokines, including IL-1β, IL-12, GM-CSF, IP-10 and MCP-1 analyzed by Luminex multiplex array (Figure 2F and Figure 2 - figure supplement 1), demonstrating that similar cytokines upregulated in human disease are expressed within the microspheres.

Extracellular matrix integrity regulates the host-pathogen interaction

In patients with TB, the host-pathogen interaction occurs in the context of the collagen-rich lung extracellular matrix (28), but most laboratory studies occur in the absence of matrix. The matrix regulates multiple facets of cell biology (2), and so to determine whether incorporation of matrix into the bio-electrospray system was a critical component of the model, we generated microspheres without collagen or with evenly distributed collagen (Figure 3A). Incorporation of type I collagen significantly reduced cell death after Mtb infection, while adherence to elastin increased cell death (Figure 3B). We therefore investigated the phenotype in microspheres containing type I collagen

141 further. PBMCs in collagen-containing microspheres had a significantly greater ability to control
142 Mtb proliferation, with lower Mtb proliferation from day 7 in the presence of collagen (Figure 3C),
143 further demonstrating that matrix integrity regulates the host-pathogen interaction.
144
145 To investigate mechanisms underlying the reduced growth in the presence of collagen, we developed
146 a multiparameter readout. Apoptosis, which is considered a host protective mechanism, was
147 increased in collagen-containing spheres compared to spheres with no collagen (Figure 3D). In
148 addition, the NADP-NADPH ratio was higher in collagen-containing spheres (Figure 3E),
149 demonstrating divergent cellular energy homeostasis. Secretion of multiple proinflammatory
150 cytokines in microspheres were increased in the presence of collagen, including IL-1β, TNF-α, IFN-γ,
151 IL-6, IL-8 and MCP-1 (Fig 3F-K). Therefore, the host-pathogen interaction is markedly different in
152 the presence of collagen, with improved control of Mtb growth, greater cell survival and altered
153 energy balance and cytokine secretion.
154
155 **Defining the role of individual cytokines**
156 An emerging paradigm within the TB field is that an optimal immune response is necessary, and that
157 either a deficit or excess of specific mediators may be deleterious from the host's perspective (8).
158 Therefore, we studied the effect of supplementing cytokines on both host and pathogen in collagen-
159 containing microspheres, investigating IFN-γ and IFN-β. Complete absence of IFN-γ leads to
160 disseminated Mtb infection in man and mouse (8), while IFN-β is of emerging importance from
161 unbiased analyses but has an undefined mechanism of action (29). Addition of exogenous IFN-β
162 resulted in a minor but significant suppression of Mtb growth (Figure 4A), whereas in contrast
163 addition of IFN-γ consistently increased growth (Figure 4B). We investigated mechanisms of this
164 divergence. Both IFN-β and IFN-γ reduced cellular toxicity in Mtb-infected microspheres (Figure 4C
165 and D). However, collagenase activity was divergently regulated, as IFN-β suppressed MMP-1
166 mRNA expression while IFN-γ increased MMP-1 expression (Fig 4E), suggesting that IFN-β has a
167 matrix-protective role. Mtb infection upregulated IL-1β, TNF-α and MCP-1 secretion, but IFN
168 augmentation did not significantly modulate this (Figure 4F, G and H). Mtb infection increased IFN-γ

169 secretion, and this was further increased by IFN-β (Figure 4I), demonstrating complex cross-talk
170 between these two cytokines.
171
172 **Investigating host-directed therapy**
173 Host-directed therapy is an emerging paradigm to improve outcome in TB infection (30). However,
174 the host immune response to Mtb has both beneficial and harmful effects, and so such therapy may
175 inadvertently drive immunopathology whilst limiting mycobacterial proliferation (14). Modulation of
176 the cyclooxygenase pathway has been proposed as a key target to limit Mtb growth (31).
177 Augmentation with exogenous PGE_2 suppressed Mtb growth in a dose-dependent manner (Figure
178 5A), consistent with findings in the mouse model of Mtb (31). The reduced Mtb luminescence
179 correlated with colony counts when microspheres were lysed and plated on Middlebrook 7H11 agar at
180 day 22 (Figure 5B). However, this improved control of bacterial growth was not without potential
181 harmful effects. Secretion of proinflammatory IL-6 and IL-8, a potent neutrophil chemoattractant,
182 was increased by PGE_2 (Figure 5C and D). Conversely, secretion of IFN-γ was suppressed by high
183 dose PGE_2 (Figure 5E). In addition, PGE_2 increased cell toxicity (Figure 5F) and suppressed total cell
184 viability (Figure 5G). PGE_2 reduced caspase 3 / 7 activity, indicating suppression of apoptosis
185 (Figure 5H). Therefore, the multiparameter readout has potential to predict protective and harmful
186 effects of host-directed therapy.
187
188 **Immunoaugmentation with Mtb-specific T cell lines**
189 The T cell response is critical to host control of Mtb but also drives pathology (32), and so a critical
190 question is which facets of the adaptive immune response are protective versus those that are
191 immunopathogenic (33). We used the tractability of the bio-electrospray model to study T cell
192 augmentation by supplementing PBMCs with autologous antigen specific T cell lines that had been
193 proliferated *ex vivo* (Figure 6 - figure supplement 1). Four days after bio-electrospraying,
194 multicellular aggregates began to form containing PBMCs, Mtb and augmented T cells (Figure 6A).
195 ESAT-6 or CFP-10 specific T cell lines, which respond to antigens secreted via the pathogenicity
196 RD1 locus, proliferated in the Mtb infected microspheres but not uninfected spheres (Figure 6B),

which was statistically significant from day 7 on quantitation (Figure 6C). Surprisingly, immunoaugmentation with either ESAT-6 or CFP-10 T cell lines led to increased Mtb growth within microspheres compared to infected PBMCs alone (Figure 6D). Augmentation with an autologous innate iNKT cell line has no effect on Mtb growth (Figure 6E), demonstrating that this was not a generic response to T cell supplementation within the microspheres. Immunoaugmentation with ESAT-6 and CFP-10 lines significantly increased secretion of multiple cytokines, including TNF-α and IL-1β into the media around microspheres (Figure 6F, 6G and Figure 6 –figure supplement 2). In contrast, augmentation did not significantly affect cell toxicity within infected microspheres (Figure 6H).

Discussion

Novel approaches to the global TB pandemic are urgently required. Mtb is an obligate human pathogen characterised by a prolonged interaction with the host (13, 34) , a spatially organised immune response (19, 20, 35) and extensive extracellular matrix turnover (28). Therefore, extended studies of human cells adherent to extracellular matrix in 3-D are likely to be essential to fully understand the host-pathogen interaction. We developed a model of human TB utilising bio-electrospray technology that replicates key features of clinical disease and optimised a multiplex readout to investigate both host and pathogen responses. We demonstrated that the extracellular matrix regulates the host immune response, consistent with reports of the ECM regulating inflammation (36), and found that collagen favours host control of Mtb. We then used the model to investigate novel therapeutic approaches. The system permitted prolonged culture of primary human cells, and we found that significant differences between experimental conditions often only emerged after more than 7 days, which would not have been observed in 2D culture systems where 3-4 days is the standard experimental duration. Our findings are consistent with other infections, where the cellular adaptions to their context determines outcome (37). This cell culture platform is highly flexible for both matrix and cellular composition within spheres and therefore has wide potential applicability within the biomedical field.

Our bioengineering approach differs significantly from traditional model systems to investigate TB, which predominantly rely on culture of human cells in 2D culture systems without extracellular matrix, infection of the zebrafish larvae with *M. marinum* or infection of mice with Mtb (16, 38, 39). The mouse model of TB has many advantages and key findings in the mouse have been replicated in man, such as critical roles for CD4+ T cells, TNF-α and IFN-γ (41), but pathology in the mouse differs from human TB (16) and humanised mice are requied to generate caseating lesions (42, 43). Other advanced human cellular models of TB have been developed. For example, Altare's group has studied a prolonged model of PBMC culture with Mtb and demonstrated cell aggregate formation (22, 23), but this model lacks extracellular matrix. A collagen matrix-containing model has been developed by Kapoor, showing aggregation and TB dormancy (24), but lacks the high throughput potential of the bioelectrospray system and rapid cellular recovery for multiparameter readouts. Generation of a complete human granuloma structure will require stromal cells such as fibroblasts, which are present in the periphery of TB granulomas (40). A key next step will be to compare patients with latent TB with active TB, and those with and without HIV-co-infection, to determine whether the model can differentiate protective immunity to Mtb directly *ex vivo*.

Many of our findings are consistent with conclusions drawn from these systems. For example, a significant role for IFN-β in the host immune response to TB is emerging from genomic studies, though it remains controversial as to whether this is protective or harmful (29). Our data suggest a predominantly protective effect, and emerging data support this conclusion (44). Similarly, we confirmed that augmentation of PGE_2 improves host control of mycobacterial proliferation, consistent with findings in the mouse (31). Finally, T cells responsive to specific Mtb antigens proliferated in infected microspheres and secreted cytokines known to be important in the host immune response to Mtb (8).

However, while some results were as expected, several findings in the 3-D system may not be predicted from current disease paradigms. For example, IFN-γ in high concentrations increases the

252 growth of TB, whereas murine experiments predict improved control. Consistent with our findings,
253 several previous studies have shown that IFN-γ increases Mtb growth in primary human cells (39, 45-
254 47). The evidence for a beneficial role of IFN-γ in humans is principally supported by individuals
255 where there is a complete absence of signalling through the IL-12/IFN pathway (48), and this
256 protective effect has clearly been shown in the mouse through both knock-out and vaccination studies
257 (41, 49). However, cohort studies have shown that a high PPD response, or high IFN-γ response to
258 ESAT-6 or CFP-10, associates with the subsequent development of TB (50-52), suggesting that an
259 excessive IFN-γ response may be deleterious. We attempted to determine if there was a tipping point
260 of IFN-γ concentration by adding IFN-γ neutralising antibodies to the microsphere matrix, and
261 although we were able to demonstrate increased growth with IFN-γ neutralisation, we found a similar
262 effect with isotype control antibodies, so it was impossible to determine if this was a specific effect.
263 Our longitudinal observations of Mtb growth in a non-destructive manner using luminescent
264 mycobacteria support the emerging concept that a balanced immune response is essential, and either a
265 deficit or excess of a specific mediator may favour the pathogen (8, 53). Combining the model with
266 CRISPR/Cas9 gene editing will permit further interrogation of each cytokine component of the
267 immune response.
268
269 PGE_2 augmentation has been proposed as a novel host-directed therapy to improve outcome in TB,
270 and we demonstrate reduced Mtb growth. However, the multiparamter analysis in our human system
271 showed that PGE_2 increases secretion of IL-8, which is likely to drive migration of neutrophils, and
272 PGE_2 also reduced host cell viability. Neutrophil recruitment has been described to have a deleterious
273 effect on host control of infection (54, 55) and therefore there is potential that this may favour Mtb,
274 driving increased pathology, lung destruction and transmission. The peak PGE_2 concentration that we
275 studied is similar to that reported in human tissue (56). We also found that immunoaugmentation
276 with ESAT-6 or CFP-10 responsive T cell lines led to increased growth of Mtb. Pathogenic
277 mycobacteria express the RD1 locus but the precise mechanism linking RD1 to pathology is not fully
278 understood (57). Our findings are consistent with the recent observations that T cell epitopes are
279 hyperconserved in pathogenic mycobacteria (58-60), indicating an evolutionary advantage to the

pathogen of specifically stimulating components of the host immune response to facilitate transmission (61). However, an alternative explanation is that the *in vitro* expansion conditions generated a T cell phenotype that was permissive to Mtb growth, skewing an initially protective phenotype to a deleterious one, and so further confirmation across different lines is required. Augmented iNKT cells did not increase Mtb growth after *ex vivo* expansion. The key conclusion of these experiments is that the immunoaugmentation model has potential to dissect protective versus pathological host immune responses.

The recent negative outcomes from both vaccine trials (10, 11) and treatment-shortening regimes (12) illustrate that observations in current model systems may not reliably translate to human disease and highlight the need for more nuanced approaches that reflect human TB infection. Our data suggest that simply driving an increased immune response to Mtb will not improve control of mycobacterial growth. Augmenting PGE_2 release by modulating the leukotriene pathway may reduce mycobacterial proliferation but may come at a cost of increased pathology. Vaccination using ESAT-6 as an antigen, which has entered human trials (62), may actually favour Mtb growth under certain circumstances, demonstrating the fine balance between the host immune response and control of pathogen growth. Critically, our data from the bioengineered model are consistent with clinical phenomena observed in human TB. For example, an excessive immune response in patients is associated with greater pulmonary pathology (32, 50, 63, 64). Similarly, our immunoaugmentation studies concur with the expression of ESAT-6 and CFP-10 by pathogenic mycobacteria, implying a critical role in causing disease (65). The model can be used to investigate approaches currently in development, such as vaccines based on targeting CD1-restricted T cells (66) and emerging host-directed therapies (67, 68), to determine whether they confer greater protection without likely harmful effects.

The bio-electrospray cell culture model has broad potential, addressing the technical complexity of performing 3-D primary cell culture within diverse extracellular matrices. The system can readily be applied to study diverse infectious and inflammatory diseases, or cancer immunotherapy, and can be

developed for high-throughput applications by combining the microsphere system with microfluidics. Integration with CRISPR/Cas9 gene editing will permit genetic manipulation of both host and pathogen (69). The multiparameter readouts define the translational potential of novel interventions over time with longitudinal data acquistion, identifying both beneficial and deleterious effects. Therefore, this system developed to dissect the host-pathogen interaction in human TB can be applied to identify novel therapeutic approaches to multiple human diseases.

Materials and Methods

Ethical approval: For analysis of blood from healthy donors and healthy TB exposed individuals, this work was approved by the National Research Ethics Service committee South Central - Southampton A, study title "An investigation into the immune response to tuberculosis infection and development of novel diagnostic markers", reference 13/SC/0043. All donors gave written informed consent. For histological analysis, samples used in this study were sourced from the Southampton Research Biorepository, University Hospital Southampton NHS Foundation Trust and University of Southampton, Mailpoint 218, Tremona Road, Southampton, SO16 6YD. Lung biopsy tissue was taken as part of routine clinical care and tissue blocks excess to diagnostic testing were analyzed in this study. The project was approved by the Institutional Review Board (Reference 12/NW/0794 SRB04_14). The ethics committee approved the analysis of this tissue without individual informed consent since it was surplus archived tissue taken as part of routine care.

PBMC cell isolation from human blood

PBMCs were isolated from single donor leukocyte cones (National Health Service Blood and Transfusion, Southampton, UK) or fresh blood from volunteers by density gradient centrifugation over Ficoll-Paque (GE Healthcare Life Sciences). These healthy donors were all recruited from a

region of very low TB incidence. For immunoaugmentation experiments requiring *Mycobacterium tuberculosis*-responsive T cells, cells from donors with a documented tuberculosis exposure were studied. All experiments were performed with primary human cells; no immortalised cell lines were used in the study.

M. tuberculosis Culture

M. tuberculosis H37Rv (Mtb) was cultured in Middlebrook 7H9 medium (supplemented with 10% ADC, 0.2% glycerol and 0.02% Tween 80) (BD Biosciences, Oxford) and bioluminescent *M. tuberculosis* H37Rv (27), GFP or mCherry expressing *M. tuberculosis* H37Rv (70) were cultured with kanamycin 25μg/ml and hygromycin 50μg/ml, respectively. Bioluminescent Mtb H37Rv was used for all experiments apart from confocal imaging. Cultures at 1x 10^8 CFU/ml Mtb (OD= 0.6) was used for all experiments at multiplicity of infection (M.O.I) of 0.1. For colony counting, Mtb was released from microspheres by EDTA/sodium citrate dissolution, cells and extracellular bacteria were pelleted by centrifugation at 3,000g, lysed with 1% saponin and then plated on Middlebrook 7H11. Colonies were counted at 3 weeks.

Cell encapsulation

Microspheres were generated with an electrostatic generator (Nisco, Zurich, Switzerland) as described previously (26). To visualise microsphere formation, a Phantom v7 high-speed camera, capable of capturing 150000 fps in conjunction with a long-distance microscope lens, was triggered simultaneously with a fibre optic lighting system to capture the jetting process. For cellular encapsulation, PBMCs were infected with Mtb overnight in a T75 flask. Cells were then detached, washed and pelleted by centrifugation at 320g and mixed with 1.5% sterile alginate (Pronova UP MVG alginate, Nova Matrix, Norway) or alginate with human collagen, fibronectin (both from Advanced BioMatrix) or human elastin (Sigma Aldrich) at a final concentration of 5 x 10^6 cells/ml. The standard matrix used in experiments was alginate-human collagen unless stated otherwise. All reagents were confirmed endotoxin free.

The cell-alginate suspension was drawn up into a sterile syringe and injected into the bead generator at 10mL/hour via a Harvard syringe driver through a 0.7-mm external diameter nozzle. Microspheres of 600µm diameter formed in an ionotropic gelling bath of 100mM $CaCl_2$ in HBSS placed below the electrostatic ring that accelerated the microspheres from the needle head. After washing twice with HBSS with Ca/Mg, microspheres were transferred in RPMI 1640 medium containing 10% of human AB serum and incubated at 37^{o}C, 21% O_2 and 5% CO_2. No media changes were performed, and supernatant was harvested at defined time points for analysis. Mtb growth within microspheres was monitored longitudinally by luminescence (GloMax® 20/20 Luminometer, Promega).

Immunofluorescence and Confocal Imaging

In specific imaging experiments, PBMCs were pre- labelled with CellTracker Blue, CellTrace™ CFSE or Hoechst 33342 (ThermoFisher Scientific, UK) according to the manufacturer recommendation. Microspheres were fixed in 4% paraformaldehyde and washed in HBSS with Ca/Mg. Confocal images were acquired on a Leica TCS SP5 Confocal microscope and processed using Image J 1.5 0d (NIH, USA).

Histological Staining and Immunohistochemistry

On day 7 and 14 of incubation, microspheres were fixed with 4% paraformaldehyde overnight and paraffin-embedded using the Shandon Cytoblock system (ThermoFisher Scientific, UK). Blocks were sectioned and stained by haematoxylin and eosin. For CD68 immunohistochemistry (Dako, Clone PG-M1), 0.5µm sections were stained. Analysis of human lung tissue taken as part of routine clinical care was approved by the Institutional Review Board (Reference 12/NW/0794 SRB04_14). Sections were dewaxed, blocked (Envision FLEX), stained with Anti-Human CD68 (Dako, Clone PG-M1), detected with HRP and counterstained with Haematoxylin.

Flow Cytometric Analysis

Cells were extracted by dissolving the microspheres in 55mM Sodium Citrate and 10mM EDTA in PBS for 10 minutes at 37°C. Cells were then suspended in PBS. Surface and intracellular staining was

done in a three-colour analysis with combinations of fluorescein isothiocyanate (FITC), phycoerythrin (PE) and allophycocyanin (APC). Antibodies used included anti-CD3, anti-CD4, anti-CD8, anti-CD14 and anti-CD68 (ImmunoTools, Germany). For T–cell proliferation, PBMCs were stained with CellTrace™ CFSE Cell Proliferation Kit for flow cytometry (ThermoFisher Scientific, UK) before infection with Mtb. Fluorescence was then analyzed by flow cytometry (BD Accuri C6 flow cytometer).

MMP-1 and IFN-γ gene expression

Microspheres were decapsulated using 55mM of sodium citrate solution and cells were lysed immediately using TRIzol Reagent (Life Technologies, Paisley, UK). 1µg RNA was reverse transcribed using High Capacity cDNA Reverse Transcription kit (Life Technologies Ltd, Paisley, UK). Taqman® Universal master mix and primers specific for GAPDH , β-Actin , MMP1, and IFN-γ gene were used for qPCR following manufacturer's instruction (Applied Biosystems, USA) and comparative threshold (CT) method was employed to analyse all qPCR data.

Luminex Analysis

Samples were sterilized by filtration through a 0.22µM Durapore membrane (Millipore) (71). Concentrations of cytokine (Life Technologies, UK) and MMP (R & D Systems, UK) were determined using a Bioplex 200 platform (Bio-Rad, UK) according to the manufacturer's protocol.

DQ Collagen Degradation Assay

For analysis of extracellular matrix degradation, microspheres were generated from a solution of 3% Alginate (Pronova UP MVG alginate, Nova Matrix, Norway), 1mg/ml of human collagen type I (Advanced BioMatrix, San Diego, California) and 100µg/ml of DQ collagen (Invitrogen, Paisley, UK). Microspheres were then placed in macrophage serum free medium (Life Technologies) and incubated at 37^{O}C. Fluorescence was read on a GloMax Discover (Promega) at an absorption maxima of 495nm and fluorescence emission maxima of 515nm.

Cell Viability Assay

Microspheres were incubated in 96-well plates at 37°C. Cell viability was analyzed using the CellTiter-Glo 3D Cell Viability Assay (Promega) according to the manufacturer's instructions, analyzing viable cells based on ATP quantitation. Luminescence was analyzed by the GloMax Discover plate reader (Promega).

Cell Toxicity Assays

CytoTox-Glo Cytotoxicity Assay (Promega) measured cellular necrosis of cells in microspheres. The kit measures dead-cell protease activity released from cells without membrane integrity using a luminogenic peptide substrate, the AAF-Glo™ Substrate. Luminescence was analyzed by GloMax Discover (Promega). Total cell death was caused by digitonin on equal cell numbers to provide the denominator. As a second measurement of toxicity, lactate dehydrogenase (LDH) release, was analyzed by a colorimetric activity assay (Roche, Burgess Hill, United Kingdom). Comparison of 2D cell culture and 3D cell culture viability was performed by plating equal numbers of cells in wells of a 96 well plate, and then measuring toxicity by LDH and CytoTox-Glo. Total toxicity was normalised to digitonin treated wells plated in parallel.

Cell Apoptosis

Microspheres were incubated in 96-well plates. Caspase-3/7 protease activities were measured as indicators of apoptosis using Apo-ONE Homogeneous Caspase-3/7 Assay (Promega) or Caspase-Glo 3/7 Assay Systems (Promega) according to the manufacturer's instructions.

NADP/NADPH ratio

The biolumiesent NADP/NADPH kit (Promega) was used according to the manufacturer's instructions.

Cytokines and PG supplementation

Microspheres were incubated in RPMI 1640 with 10% AB serum with IFN-β, IFN-γ (eBioscience) or PGE_2 (R&D Systems) at 37°C.

Immunoaugmentation with autologous T Cells

To generate expanded specific T cell lines, ESAT-6 or CFP-10 specific cells were derived from PBMCs from Mtb-exposed individuals (72). Monocytes were isolated from PBMCs using magnetic cell separation (Miltenyi Biotec, UK) and partially differentiated into monocyte derived dendritic cells (moDCs) for 3 days using complete media supplemented with GM-CSF (20ng/ml) and IL-4 (25ng/ml). moDCs were then loaded with peptide antigen pools derived from ESAT-6 or CFP-10 proteins in the presence of IFN-γ and LPS. moDCs were then exposed to $CD14^-$ T cell fractions in a 1:2 ratio for 7 days, after which IL-2 (400IU/ml, Proleukin, Chiron), IL-15 (2ng/ml) and IL-7 (2ng/ml, Immunotools) were added. T-cell specificity was confirmed by IFN-γ secretion upon exposure of T-cells to autologous moDCs loaded with CFP-10 or ESAT-6. Human iNK T cells were derived from PBMCs according to the method previously described (73). Briefly, iNK T cell lines were generated by incubating PBMCs with 200ng/ml KRN7000 (AXXORA) for 7 days before the addition of IL-2, IL-7 and IL-15. After 2 weeks culture, iNK T cell expansion was confirmed via CD3, Va24 and CD1d-K7 tetramer staining. Cells were acquired using FACSAria (Becton Dickinson, UK). ESAT-6, CFP-10 specific T cell lines or iNK T cells were counted and then PBMCs were supplemented with 20% additional immunoaugmented cells immediately prior to Mtb infection. After overnight incubation, the combined cells were bioelectrosprayed by our standard protocol.

Statistical analysis

All experiments were performed a minimum of 2 occasions from separate donors as biological replicates and on each occasion with a minimum of 3 technical replicates. Data presented are from a representative donor and include the mean and SEM. Analysis was performed in Graphpad Prism v6.0. Students t-test was used to compare pairs and ANOVA for groups of 3 or more.

Acknowledgements

This work was supported by the US National Institute for Health R33AI102239, the UK National Centre for the 3Rs NC/L001039/1 and the Antimicrobial Resistance Cross Council Initiative supported by the seven research councils MR/N006631/1. We would like to thank Jennifer Russell and Regina Teo, University of Southampton, for excellent technical assistance. We thank Nuria Andreu and Siouxsie Wiles for providing the Lux-expressing Mtb, Brian Robertson for the GFP+ Mtb and Tanya Parish for the mCherry expressing Mtb. The authors declare no conflict of interest.

References

1. Benam KH, Dauth S, Hassell B, Herland A, Jain A, Jang KJ, et al. Engineered in vitro disease models. Annu Rev Pathol. 2015;10:195-262.

2. Pampaloni F, Reynaud EG, Stelzer EH. The third dimension bridges the gap between cell culture and live tissue. Nat Rev Mol Cell Biol. 2007;8(10):839-45.

3. Yamada KM, Cukierman E. Modeling tissue morphogenesis and cancer in 3D. Cell. 2007;130(4):601-10.

4. Schwartz MA, Chen CS. Cell biology. Deconstructing dimensionality. Science. 2013;339(6118):402-4.

5. Parker MW, Rossi D, Peterson M, Smith K, Sikstrom K, White ES, et al. Fibrotic extracellular matrix activates a profibrotic positive feedback loop. J Clin Invest. 2014;124(4):1622-35.

6. Cheng F, Pekkonen P, Laurinavicius S, Sugiyama N, Henderson S, Gunther T, et al. KSHV-initiated notch activation leads to membrane-type-1 matrix metalloproteinase-dependent lymphatic endothelial-to-mesenchymal transition. Cell Host Microbe. 2011;10(6):577-90.

7. Barrila J, Radtke AL, Crabbe A, Sarker SF, Herbst-Kralovetz MM, Ott CM, et al. Organotypic 3D cell culture models: using the rotating wall vessel to study host-pathogen interactions. Nat Rev Microbiol. 2010;8(11):791-801.

8. O'Garra A, Redford PS, McNab FW, Bloom CI, Wilkinson RJ, Berry MP. The immune response in tuberculosis. Annu Rev Immunol. 2013;31:475-527.

9. Horsburgh CR, Jr., Barry CE, 3rd, Lange C. Treatment of Tuberculosis. N Engl J Med. 2015;373(22):2149-60.

10. Tameris MD, Hatherill M, Landry BS, Scriba TJ, Snowden MA, Lockhart S, et al. Safety and efficacy of MVA85A, a new tuberculosis vaccine, in infants previously vaccinated with BCG: a randomised, placebo-controlled phase 2b trial. Lancet. 2013;381(9871):1021-8.

11. Ndiaye BP, Thienemann F, Ota M, Landry BS, Camara M, Dieye S, et al. Safety, immunogenicity, and efficacy of the candidate tuberculosis vaccine MVA85A in healthy adults

495 infected with HIV-1: a randomised, placebo-controlled, phase 2 trial. The lancet Respiratory
496 medicine. 2015;3(3):190-200.
497 12. Warner DF, Mizrahi V. Shortening treatment for tuberculosis--to basics. N Engl J Med.
498 2014;371(17):1642-3.
499 13. Russell DG. Mycobacterium tuberculosis and the intimate discourse of a chronic infection.
500 Immunol Rev. 2011;240(1):252-68.
501 14. Elkington PT, Friedland JS. Permutations of time and place in tuberculosis. Lancet Infect Dis.
502 2015;15(11):1357-60.
503 15. Seok J, Warren HS, Cuenca AG, Mindrinos MN, Baker HV, Xu W, et al. Genomic responses
504 in mouse models poorly mimic human inflammatory diseases. Proc Natl Acad Sci U S A.
505 2013;110(9):3507-12.
506 16. Young D. Animal models of tuberculosis. Eur J Immunol. 2009;39(8):2011-4.
507 17. Buchheit CL, Rayavarapu RR, Schafer ZT. The regulation of cancer cell death and
508 metabolism by extracellular matrix attachment. Seminars in cell & developmental biology.
509 2012;23(4):402-11.
510 18. Mueller-Klieser W. Three-dimensional cell cultures: from molecular mechanisms to clinical
511 applications. Am J Physiol. 1997;273(4 Pt 1):C1109-23.
512 19. Marakalala MJ, Raju RM, Sharma K, Zhang YJ, Eugenin EA, Prideaux B, et al. Inflammatory
513 signaling in human tuberculosis granulomas is spatially organized. Nat Med. 2016;22(5):531-8.
514 20. Mattila JT, Ojo OO, Kepka-Lenhart D, Marino S, Kim JH, Eum SY, et al. Microenvironments
515 in tuberculous granulomas are delineated by distinct populations of macrophage subsets and
516 expression of nitric oxide synthase and arginase isoforms. J Immunol. 2013;191(2):773-84.
517 21. Al Shammari B, Shiomi T, Tezera L, Bielecka MK, Workman V, Sathyamoorthy T, et al. The
518 Extracellular Matrix Regulates Granuloma Necrosis in Tuberculosis. J Infect Dis. 2015;212(3):463-
519 73.
520 22. Puissegur MP, Botanch C, Duteyrat JL, Delsol G, Caratero C, Altare F. An in vitro dual
521 model of mycobacterial granulomas to investigate the molecular interactions between mycobacteria
522 and human host cells. Cell Microbiol. 2004;6(5):423-33.

23. Lay G, Poquet Y, Salek-Peyron P, Puissegur MP, Botanch C, Bon H, et al. Langhans giant cells from M. tuberculosis-induced human granulomas cannot mediate mycobacterial uptake. J Pathol. 2007;211(1):76-85.

24. Kapoor N, Pawar S, Sirakova TD, Deb C, Warren WL, Kolattukudy PE. Human Granuloma In Vitro Model, for TB Dormancy and Resuscitation. PLoS ONE. 2013;8(1):e53657.

25. Parasa VR, Rahman MJ, Ngyuen Hoang AT, Svensson M, Brighenti S, Lerm M. Modeling Mycobacterium tuberculosis early granuloma formation in experimental human lung tissue. Dis Model Mech. 2014;7(2):281-8.

26. Workman VL, Tezera LB, Elkington PT, Jayasinghe SN. Controlled Generation of Microspheres Incorporating Extracellular Matrix Fibrils for Three-Dimensional Cell Culture. Adv Funct Mater. 2014;24(18):2648-57.

27. Andreu N, Zelmer A, Fletcher T, Elkington PT, Ward TH, Ripoll J, et al. Optimisation of bioluminescent reporters for use with mycobacteria. PLoS ONE. 2010;5(5):e10777.

28. Elkington PT, D'Armiento JM, Friedland JS. Tuberculosis immunopathology: the neglected role of extracellular matrix destruction. Sci Transl Med. 2011;3(71):71ps6.

29. Cliff JM, Kaufmann SH, McShane H, van Helden P, O'Garra A. The human immune response to tuberculosis and its treatment: a view from the blood. Immunol Rev. 2015;264(1):88-102.

30. Hawn TR, Shah JA, Kalman D. New tricks for old dogs: countering antibiotic resistance in tuberculosis with host-directed therapeutics. Immunol Rev. 2015;264(1):344-62.

31. Mayer-Barber KD, Andrade BB, Oland SD, Amaral EP, Barber DL, Gonzales J, et al. Host-directed therapy of tuberculosis based on interleukin-1 and type I interferon crosstalk. Nature. 2014;511(7507):99-103.

32. Kaufmann SH, Dorhoi A. Inflammation in tuberculosis: interactions, imbalances and interventions. Curr Opin Immunol. 2013;25(4):441-9.

33. Jasenosky LD, Scriba TJ, Hanekom WA, Goldfeld AE. T cells and adaptive immunity to Mycobacterium tuberculosis in humans. Immunol Rev. 2015;264(1):74-87.

34. Cambier CJ, Falkow S, Ramakrishnan L. Host evasion and exploitation schemes of Mycobacterium tuberculosis. Cell. 2014;159(7):1497-509.

551 35. Egen JG, Rothfuchs AG, Feng CG, Winter N, Sher A, Germain RN. Macrophage and T Cell
552 Dynamics during the Development and Disintegration of Mycobacterial Granulomas. Immunity.
553 2008;28(2):271-84.
554 36. Sorokin L. The impact of the extracellular matrix on inflammation. Nat Rev Immunol.
555 2010;10(10):712-23.
556 37. Snijder B, Sacher R, Ramo P, Damm EM, Liberali P, Pelkmans L. Population context
557 determines cell-to-cell variability in endocytosis and virus infection. Nature. 2009;461(7263):520-3.
558 38. Guirado E, Schlesinger LS. Modeling the Mycobacterium tuberculosis Granuloma - the
559 Critical Battlefield in Host Immunity and Disease. Frontiers in immunology. 2013;4:98.
560 39. Vogt G, Nathan C. In vitro differentiation of human macrophages with enhanced
561 antimycobacterial activity. J Clin Invest. 2011;121(10):3889-901.
562 40. O'Kane CM, Elkington PT, Jones MD, Caviedes L, Tovar M, Gilman RH, et al. STAT3, p38
563 MAPK, and NF-kappaB drive unopposed monocyte-dependent fibroblast MMP-1 secretion in
564 tuberculosis. Am J Respir Cell Mol Biol. 2010;43(4):465-74.
565 41. Flynn JL, Chan J. Immunology of tuberculosis. Annu Rev Immunol. 2001;19:93-129.
566 42. Calderon VE, Valbuena G, Goez Y, Judy BM, Huante MB, Sutjita P, et al. A humanized
567 mouse model of tuberculosis. PLoS ONE. 2013;8(5):e63331.
568 43. Heuts F, Gavier-Widen D, Carow B, Juarez J, Wigzell H, Rottenberg ME. CD4+ cell-
569 dependent granuloma formation in humanized mice infected with mycobacteria. Proc Natl Acad Sci U
570 S A. 2013;110(16):6482-7.
571 44. Moreira-Teixeira L, Sousa J, McNab FW, Torrado E, Cardoso F, Machado H, et al. Type I
572 IFN Inhibits Alternative Macrophage Activation during Mycobacterium tuberculosis Infection and
573 Leads to Enhanced Protection in the Absence of IFN-gamma Signaling. J Immunol.
574 2016;197(12):4714-26.
575 45. Douvas GS, Looker DL, Vatter AE, Crowle AJ. Gamma interferon activates human
576 macrophages to become tumoricidal and leishmanicidal but enhances replication of macrophage-
577 associated mycobacteria. Infect Immun. 1985;50(1):1-8.

578 46. Rook GA, Steele J, Ainsworth M, Champion BR. Activation of macrophages to inhibit
579 proliferation of Mycobacterium tuberculosis: comparison of the effects of recombinant gamma-
580 interferon on human monocytes and murine peritoneal macrophages. Immunology. 1986;59(3):333-8.
581 47. Crowle AJ, Elkins N. Relative permissiveness of macrophages from black and white people
582 for virulent tubercle bacilli. Infect Immun. 1990;58(3):632-8.
583 48. Karp CL, Wilson CB, Stuart LM. Tuberculosis vaccines: barriers and prospects on the quest
584 for a transformative tool. Immunol Rev. 2015;264(1):363-81.
585 49. Aagaard C, Hoang T, Dietrich J, Cardona PJ, Izzo A, Dolganov G, et al. A multistage
586 tuberculosis vaccine that confers efficient protection before and after exposure. Nat Med.
587 2011;17(2):189-94.
588 50. Comstock GW, Livesay VT, Woolpert SF. The prognosis of a positive tuberculin reaction in
589 childhood and adolescence. American journal of epidemiology. 1974;99(2):131-8.
590 51. Higuchi K, Harada N, Fukazawa K, Mori T. Relationship between whole-blood interferon-
591 gamma responses and the risk of active tuberculosis. Tuberculosis (Edinb). 2008;88(3):244-8.
592 52. del Corral H, Paris SC, Marin ND, Marin DM, Lopez L, Henao HM, et al. IFNgamma
593 response to Mycobacterium tuberculosis, risk of infection and disease in household contacts of
594 tuberculosis patients in Colombia. PLoS One. 2009;4(12):e8257.
595 53. Gideon HP, Phuah J, Myers AJ, Bryson BD, Rodgers MA, Coleman MT, et al. Variability in
596 Tuberculosis Granuloma T Cell Responses Exists, but a Balance of Pro- and Anti-inflammatory
597 Cytokines Is Associated with Sterilization. PLoS Pathog. 2015;11(1):e1004603.
598 54. Kimmey JM, Huynh JP, Weiss LA, Park S, Kambal A, Debnath J, et al. Unique role for
599 ATG5 in neutrophil-mediated immunopathology during M. tuberculosis infection. Nature.
600 2015;528(7583):565-9.
601 55. Nouailles G, Dorhoi A, Koch M, Zerrahn J, Weiner J, 3rd, Fae KC, et al. CXCL5-secreting
602 pulmonary epithelial cells drive destructive neutrophilic inflammation in tuberculosis. J Clin Invest.
603 2014;124(3):1268-82.

56. Reikeras O, Helle A, Krohn CD, Brox JI. Effects of high-dose corticosteroids on post-traumatic inflammatory mediators. Inflammation research : official journal of the European Histamine Research Society [et al]. 2009;58(12):891-7.

57. Majlessi L, Prados-Rosales R, Casadevall A, Brosch R. Release of mycobacterial antigens. Immunol Rev. 2015;264(1):25-45.

58. Comas I, Chakravartti J, Small PM, Galagan J, Niemann S, Kremer K, et al. Human T cell epitopes of Mycobacterium tuberculosis are evolutionarily hyperconserved. Nat Genet. 2010;42(6):498-503.

59. Coscolla M, Copin R, Sutherland J, Gehre F, de Jong B, Owolabi O, et al. M. tuberculosis T Cell Epitope Analysis Reveals Paucity of Antigenic Variation and Identifies Rare Variable TB Antigens. Cell Host Microbe. 2015;18(5):538-48.

60. Lindestam Arlehamn CS, Paul S, Mele F, Huang C, Greenbaum JA, Vita R, et al. Immunological consequences of intragenus conservation of Mycobacterium tuberculosis T-cell epitopes. Proc Natl Acad Sci U S A. 2015;112(2):E147-55.

61. Orme IM, Robinson RT, Cooper AM. The balance between protective and pathogenic immune responses in the TB-infected lung. Nat Immunol. 2015;16(1):57-63.

62. Luabeya AK, Kagina BM, Tameris MD, Geldenhuys H, Hoff ST, Shi Z, et al. First-in-human trial of the post-exposure tuberculosis vaccine H56:IC31 in Mycobacterium tuberculosis infected and non-infected healthy adults. Vaccine. 2015;33(33):4130-40.

63. Philips JA, Ernst JD. Tuberculosis pathogenesis and immunity. Annu Rev Pathol. 2012;7:353-84.

64. Nunes-Alves C, Booty MG, Carpenter SM, Jayaraman P, Rothchild AC, Behar SM. In search of a new paradigm for protective immunity to TB. Nat Rev Microbiol. 2014;12(4):289-99.

65. Brites D, Gagneux S. Co-evolution of Mycobacterium tuberculosis and Homo sapiens. Immunol Rev. 2015;264(1):6-24.

66. Van Rhijn I, Moody DB. CD1 and mycobacterial lipids activate human T cells. Immunol Rev. 2015;264(1):138-53.

631 67. Hawn TR, Matheson AI, Maley SN, Vandal O. Host-directed therapeutics for tuberculosis:
632 can we harness the host? Microbiology and molecular biology reviews : MMBR. 2013;77(4):608-27.
633 68. Zumla A, Chakaya J, Hoelscher M, Ntoumi F, Rustomjee R, Vilaplana C, et al. Towards host-
634 directed therapies for tuberculosis. Nat Rev Drug Discov. 2015;14(8):511-2.
635 69. Chakraborty S, Ji H, Kabadi AM, Gersbach CA, Christoforou N, Leong KW. A
636 CRISPR/Cas9-based system for reprogramming cell lineage specification. Stem Cell Reports.
637 2014;3(6):940-7.
638 70. Carroll P, Schreuder LJ, Muwanguzi-Karugaba J, Wiles S, Robertson BD, Ripoll J, et al.
639 Sensitive Detection of Gene Expression in Mycobacteria under Replicating and Non-Replicating
640 Conditions Using Optimized Far-Red Reporters. PLoS ONE. 2010;5(3):e9823.
641 71. Elkington PT, Green JA, Friedland JS. Filter sterilization of highly infectious samples to
642 prevent false negative analysis of matrix metalloproteinase activity. J Immunol Methods. 2006;309(1-
643 2):115-9.
644 72. Wölfl M, Greenberg PD. Antigen-specific activation and cytokine-facilitated expansion of
645 naive, human CD8+ T cells. Nat Protocols. 2014;9(4):950-66.
646 73. Mansour S, Tocheva AS, Sanderson JP, Goulston LM, Platten H, Serhal L, et al. Structural
647 and Functional Changes of the Invariant NKT Clonal Repertoire in Early Rheumatoid Arthritis. The
648 Journal of Immunology. 2015;195(12):5582-91.

649

650 # Figure legends

651

652 **Figure 1: Primary human cells have greater survival in 3-D and aggregate, differentiate and**
653 **fuse into multinucleate giant cells. A.** Phase contrast microscopy with overlay of Hoeschst 33256
654 (blue) at Day 7 demonstrates PBMCs forming aggregates within microspheres. Scale 300µm. **B.** Cell
655 aggregation in Mtb-infected PBMC-collagen-alginate microspheres at Day 7. Scale 50µm. **C.** Cell
656 aggregation is greater in Mtb-infected microspheres than uninfected microspheres. Cells aggregates
657 were defined as 8 or more cells viewed under 20x magnification. Data are representative of a
658 minimum of 10 fields of view per group. **D.** Cells were infected with GFP+ Mtb and then released by
659 decapsulation. At 24h after infection, 24.2% monocytes had phagocytosed GFP-expressing Mtb by
660 flow cytometric analysis. **E.** Haematoxylin and eosin staining of paraffin-fixed microspheres
661 demonstrates cell aggregates in Mtb-infected microspheres at day 14. Scale 20µm. **F.** Host cell
662 survival is significantly greater in 3-D microspheres than 2-D cell culture as demonstrated by LDH
663 assay. Clear box 2-D cell culture, filled box 3-D culture; an equal number of cells killed with
664 digitonin (30µg/ml) in the respective 3D and 2D culture was used as denominator. Mean ± SE values
665 (n=4). **G.** Cytotoxicity measured by CytoTox Glo assay is significantly lower in 3D culture than 2D
666 culture. **H.** CD68 expression is increased in macrophages in Mtb-infected microspheres analyzed
667 by flow cytometry. Black isotype control, blue uninfected cells, red Mtb-infected cells. **I.**
668 Multinucleate giant cells form within microspheres at day 14, immunostained with CD68 (brown) and
669 counterstained with Haematoxylin (blue). Scale 20µm. **J.** In patients with pulmonary TB, similar
670 giant cells are observed in pulmonary granulomas. Low power image of human pulmonary
671 granuloma (G), with numerous multinucleate giant cells surrounding caseous centre (box, magnified
672 area). Scale bar: 1000µm.

673

674 **Figure 2: Mtb grows within microspheres containing PBMCs and upregulates MMP and**
675 **cytokine expression. A.** Mtb proliferates slowly in microspheres with no cells (green line), but
676 progressively in microspheres containing PBMCs (red line), reaching similar luminescence to
677 Middlebrook 7H9 broth culture at 24 days (black line). Blue line, uninfected microspheres. **B.** Mtb

infection upregulates MMP-1 gene expression and **(C)** MMP-9 secretion in microspheres. **D.** MMP upregulation has a functional effect, causing collagen degradation. DQ Collagen breakdown is higher in Mtb-infected microspheres (red line) than uninfected (blue line). Triangles, microspheres with no PBMCs. **E.** Mtb infection increases cellular IFN-γ mRNA accumulation relative to uninfected cells at day 4 in microspheres (n=4). **F**. Secretion of cytokines by Mtb-infected microspheres (squares) is significantly higher than in microspheres containing uninfected PBMCs (circles). ****p< 0.0001 by t-test (B and E) and ANOVA (A, C, D, F).

Figure 3: Incorporation of collagen into microspheres limits Mtb growth and increases host cell survival. A. Microspheres were created without collagen (i), or incorporating FITC-labelled collagen (ii) to demonstrate distribution. Immediately after bioelectrospraying, collagen is homogenous throughout the microspheres. **B.** Incorporation of Type I collagen into microspheres improves cell survival at 72h after Mtb infection, whereas elastin did not, analyzed by CytoTox-Glo assay. **C.** PBMCs control Mtb growth in microspheres containing collagen (squares) better than cells without collagen (circles). Open squares, uninfected PBMCs. **D.** The level of apoptosis and NADP+/NADPH ratio (**E**) are higher in microspheres containing collagen at day 7. Collagen incorporation caused increased secretion of IL-1β (**F**), TNF-α (**G**), IFN-γ (**H**), IL-6 (**I**), MCP-1 (**J**) and IL-8 (**K**) at day 7. Each experiment was performed a minimum of 2 times and charts represent mean values + SEM of a representative experiment performed in triplicate. * p< 0.05, **p<0.01, ***p< 0.001, ****p< 0.0001.

Figure 4: IFN-β and IFN-γ have divergent effects on bacterial growth within microspheres. A. Exogenous IFN-β suppresses Mtb growth after 24 days culture. Black line represents Mtb infected PBMCs. IFN-β supplementation at 0.02nM (blue), 0.2nM (green) and 2nM (red) suppresses Mtb luminescence. **B.** IFN-γ increases Mtb growth compared to infected PBMCs without additional cytokine. Exogenous IFN-γ at 0.02nM (blue), 0.2nM (green) and 2nM (red) increases Mtb

luminescence above Mtb-infected PBMCs without cytokine supplementation (black line). **C, D.** Both IFN-β and IFN-γ reduce toxicity in Mtb-infected PBMCs, analyzed by CytoTox-Glo assay. **E.** IFNs divergently regulate MMP-1, with IFN-β suppressing gene expression in infected microspheres while IFN-γ increases MMP-1 expression. **F-H**. Mtb upregulates cytokine secretion but this is not modulated by IFNs. IFN-β drives TNF-α and MCP-1 as a single stimulus (E and G), but has no significant synergistic effect with Mtb. **I.** Mtb upregulates IFN-γ secretion, and this is further increased by addition of IFN-β. Mean + SEM of a representative experiment performed in triplicate is shown, and are representative of a minimum of 2 experiments done in triplicate. * $p< 0.05$, **$p<0.01$, ***$p< 0.001$ and ****$p< 0.0001$.

Figure 5: PGE_2 augmentation limits bacterial growth but increases pro-inflammatory cytokine secretion and cellular toxicity. A. Addition of exogenous PGE_2 suppresses Mtb growth in microspheres in a dose-dependent manner. Mtb-infected PBMCs (black line), 0.2µg/ml PGE_2 (green line), 2µg/ml PGE_2 (red line), 20µg/ml PGE_2 (blue line). **B.** Colony counts of microspheres decapsulated at day 24 and then plated on Middlebrook 7H11 agar correlate with luminescence. **C, D and E.** PGE_2 increases secretion of IL-6 and IL-8, but significantly decreases IFN-γ secretion, from Mtb-infected microspheres. **F.** Cellular toxicity is increased in PGE_2 treated microspheres at day 3, analyzed by LDH release, and (**G**) total cell viability was reduced at day 7, analyzed by CytoTox-Glo assay. **H.** PGE_2 reduces caspase 3/7 activity at day 7. *$p< 0.05$, **$p<0.01$, ***$p< 0.001$.

Figure 6: Immunoaugmentation with Mtb-specific T cells increases Mtb growth. A. Microspheres imaged after 4 days show early granuloma formation. (i) PBMCs labelled with CellTrace™ CFSE (green), (ii) Mtb expressing mCherry (red), (iii) autologous ESAT-6 specific T cells labelled with CellTracker Blue, (iv) Merged image shows granulomas containing Mtb, PBMCs and augmented T cells (yellow). **B.** Cellular proliferation is increased in infected microspheres with immunoaugmented autologous T cells, analysed by CFSE staining. Day 1, black line; Day 7, red line;

730 (i) Uninfected, (ii) Mtb-infected. **C.** Quantitative analysis of the proliferative capacity of ESAT-6
731 augumented PBMCs at Day 1 and Day 7. The bars show percentage of proliferating CD4 cells after
732 gating on CD3+CD4+ lymphocytes. Differences between Day 1 and 7 were assessed for three
733 experiments by t-test. **D.** Addition of either ESAT-6 responsive T cells (red) or CFP-10 responsive T
734 cells (blue) increases Mtb growth compared to infected PBMCs without supplemented T cells (black).
735 Open symbols, uninfected microspheres. **E.** Supplementation with an iNKT autologous T cell line
736 (blue triangle) did not significantly affect Mtb growth compared to infected PBMCs alone (black
737 square). **F, G.** Secretion of TNF-α and IL-1β is increased in immunoaugmented microspheres at day
738 7. **H.** Immunoaugmentation did not significantly modulate cell toxicity in infected microspheres at
739 day 3 analysed by LDH release.

740

741

Supplementary figures

Figure 1 - Supplementary figure 1: Equipment set-up within containment level 3 tuberculosis laboratory. **A.** Bioelectrosprayer housed within a double sized class I/III Microbiological Safety Cabinet. **B.** Close-up of the bioelectrosprayer cleaned after an experiment, with syringe driver on top. The external doors must be closed for microsphere generation to commence, providing the first level of containment, with the airflow of the class I MSC providing the second level of containment. The cabinet is formalin-fumigated after each experiment.

Figure 1 - Supplementary figure 2: Microspheres placed in a 12 well tissue culture plate immediately after generation demonstrating non-magnified appearance.

Figure 1 - Supplementary figure 3: Medium viscosity guluronate (MVG) alginate is the optimal alginate for immunological studies. **A.** IL-8 secretion from microspheres composed of different alginates measured by ELISA. MVM: medium viscosity mannuronate, LVG: low viscosity guluronate. In addition, LVG had very poor biophysical properties for biolelectrospraying. **B.** Cell viability analyzed by LDH release was not different between the different alginate types. **C.** In sterile alginate, IL-8 secretion was higher in microspheres containing SLG compared to SLM. SLG: Sterile guluronate, SLM: sterile mannuronate. Squares, filled lines: Mtb-infected microspheres, circles and broken lines: uninfected microspheres.

Figure 1 - Supplementary figure 4: Viability of PBMCs remains over 90% after decapsulation. PBMCs were encapsulated into alginate-collagen microspheres. After 1 hr incubation at 37^{o}C in HBSS , they were decapsulated in solution of 55mM of sodium citrate and 5mM EDTA prepared in HBSS (pH=7.4) for 10 minutes. The cells were then washed with HBSS twice before suspension in 5 ml of RPMI and staining with propidium iodide (1mg/ml) at 1:100 dilution and analysis by flow

cytometry. For comparison, viability of PBMCs kept in RPMI at 4^{o}C during this period was used. Data is a representative of two independent experiments.

Figure 1 - Supplementary figure 5: T cell composition of microspheres. The proportion of CD4+ T cells increases between day 0 and day 7 in both uninfected and infected microspheres (A), while the proportion of CD8+ T cells falls (B). * p< 0.05, **p<0.01, ***p< 0.001, ****p< 0.0001 compared to day 0.

Figure 2 - Supplementary figure 1: Mtb infection upregulates secretion of multiple growth factors, cytokines and chemokines from microspheres measured by Luminex array. * p< 0.05, **p<0.01, ***p< 0.001, ****p< 0.0001 compared to uninfected microspheres at each time point.

Figure 6 - Supplementary figure 1: Confirmation of specificity of *in vitro* expanded T cells. **A.** Dot plot shows percentage of T cells that are either CD4+/CD8+, CD4+/CD8-, CD4-/CD8+, CD4-/CD8- from ESAT-6 (i) and CFP-10 (ii) specific T cell lines. **B.** PBMC were cultured with ESAT-6 (i) and CFP-10 (ii) peptides and after two weeks' culture, T cell specificity was confirmed by IFN-γ release after exposure to their respective antigen. The iNKT antigen KRN7000 was used as a negative control and PMA/Ionomycin as a polyclonal T cell mitogen. Data is representative of three donors with each co-culture performed in triplicate. **C.** Percentage of ESAT-6 (i) and CFP-10 (ii) specific T cells measured by intracellular cytokine staining. Monocyte derived dendritic cells (moDCs) were pulsed with ESAT-6 or CFP-10 peptide for 12 hours prior to the addition of T cells. After 8 hours of stimulation with their corresponding antigen, each line was stained for intracellular cytokines and cells were acquired on a FACSaria. **D.** Dot plots representing *in vitro* antigen induced iNKT expansion in one donor. Live CD3+ CD1d-K7 tet+ Vα24 + iNKT cells were stained (i) *ex vivo* and (ii) 2 weeks post stimulation with KRN7000. Plots show % of iNKT cells ex vivo (0.68%) and after in vitro culture (71.1%) confirming their expansion.

Figure 6 - Supplementary figure 2: Augmentation of PBMCs with ESAT-6/CFP-10 specific T cell lines in microspheres causes differential secretion of cytokines after Mtb infection compared to PBMCs alone. **(A-D)** Cytokine secretion in CFP-10 and ESAT-6 specific T cell supplemented microspheres was normalized to the secretion from infected PBMCs within PBMC-only microspheres and results are expressed as relative units. **(E)** Graphic representation of the cytokine profile (n=3). Data show mean ± SEM of three independent experiments done in triplicate. *p<0.05, **p<0.01, ***p<0.001, p<0.0001.

Video Legend

Supplementary video 1: Generation of microspheres. During the bio-electrospray process, a Phantom v7 high-speed camera, capable of capturing 150000 fps in conjunction with a long-distance microscope lens, was triggered simultaneously with a fibre optic lighting system. Relative video speed 0.15s.

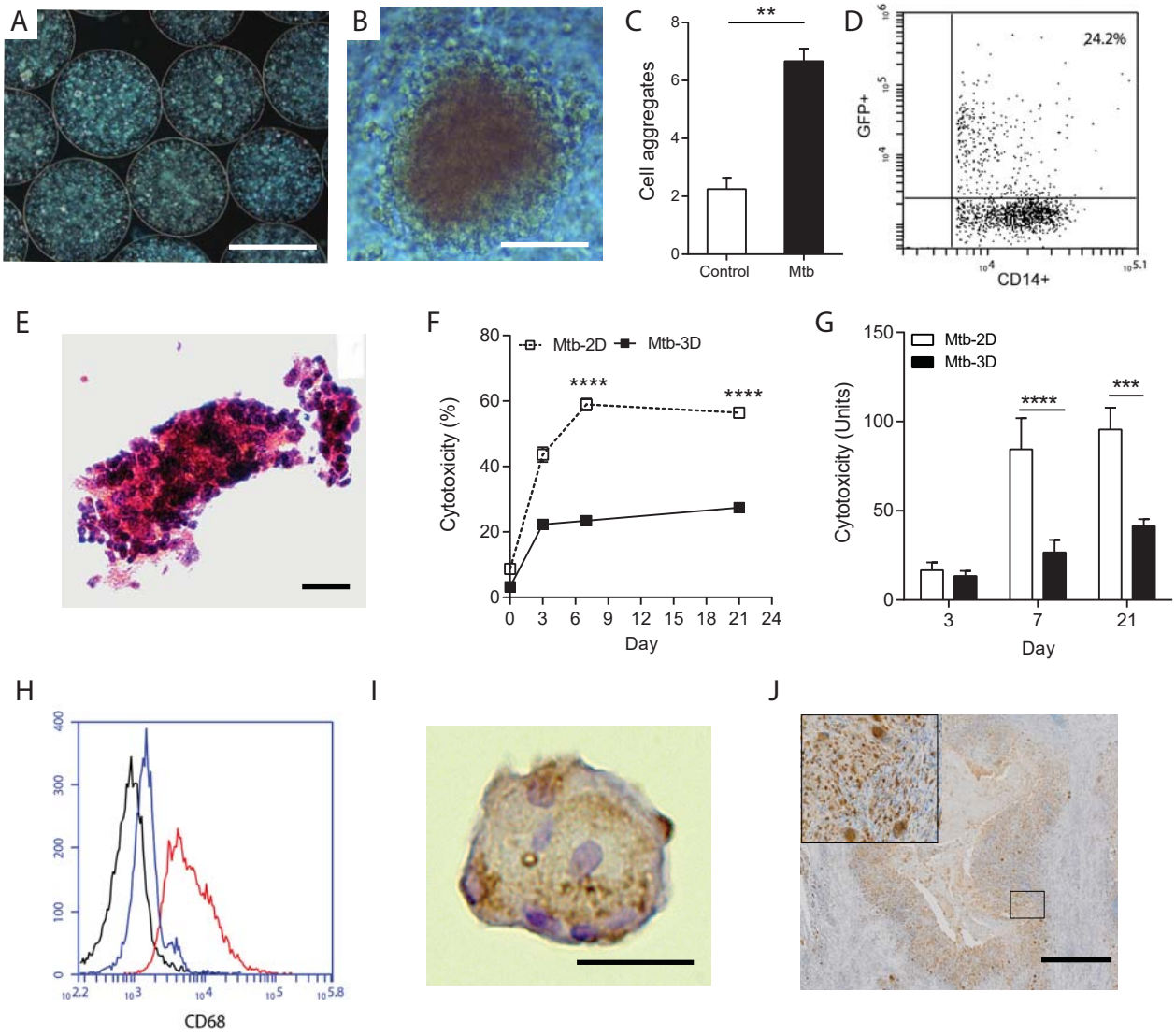

Figure 1: Primary human cells have greater survival in 3-D and aggregate, differentiate and fuse into multinucleate giant cells. **A.** Phase contrast microscopy with overlay of Hoeschst 33256 (blue) at Day 7 demonstrates PBMCs forming aggregates within microspheres. Scale 300µm. **B.** Cell aggregation in Mtb-infected PBMC-collagen-alginate microspheres at Day 7. Scale 50µm. **C.** Cell aggregation is greater in Mtb-infected microspheres than uninfected microspheres. Cells aggregates were defined as 8 or more cells viewed under 20x magnification. Data are representative of a minimum of 10 fields of view per group. **D.** Cells were infected with GFP+ Mtb and then released by decapsulation. At 24h after infection, 24.2% monocytes had phagocytosed GFP-expressing Mtb by flow cytometric analysis. **E.** Haematoxylin and eosin staining of paraffin-fixed microspheres demonstrates cell aggregates in Mtb-infected microspheres at day 14. Scale 20µm. **F.** Host cell survival is significantly greater in 3-D microspheres than 2-D cell culture as demonstrated by LDH assay. Clear box 2-D cell culture, filled box 3-D culture; an equal number of cells killed with digitonin (30µg/ml) in the respective 3D and 2D culture was used as denominator. Mean ± SE values (n=4). **G.** Cytotoxicity measured by CytoTox Glo assay is significantly lower in 3D culture than 2D culture. **H.** CD68 expression is increased in macrophages in Mtb-infected microspheres analyzed by flow cytometry. Black isotype control, blue uninfected cells, red Mtb-infected cells. **I.** Multinucleate giant cells form within microspheres at day 14, immunostained with CD68 (brown) and counterstained with Haematoxylin (blue). Scale 20µm. **J.** In patients with pulmonary TB, similar giant cells are observed in pulmonary granulomas. Low power image of human pulmonary granuloma (G), with numerous multinucleate giant cells surrounding caseous centre (box, magnified area). Scale bar: 1000µm.

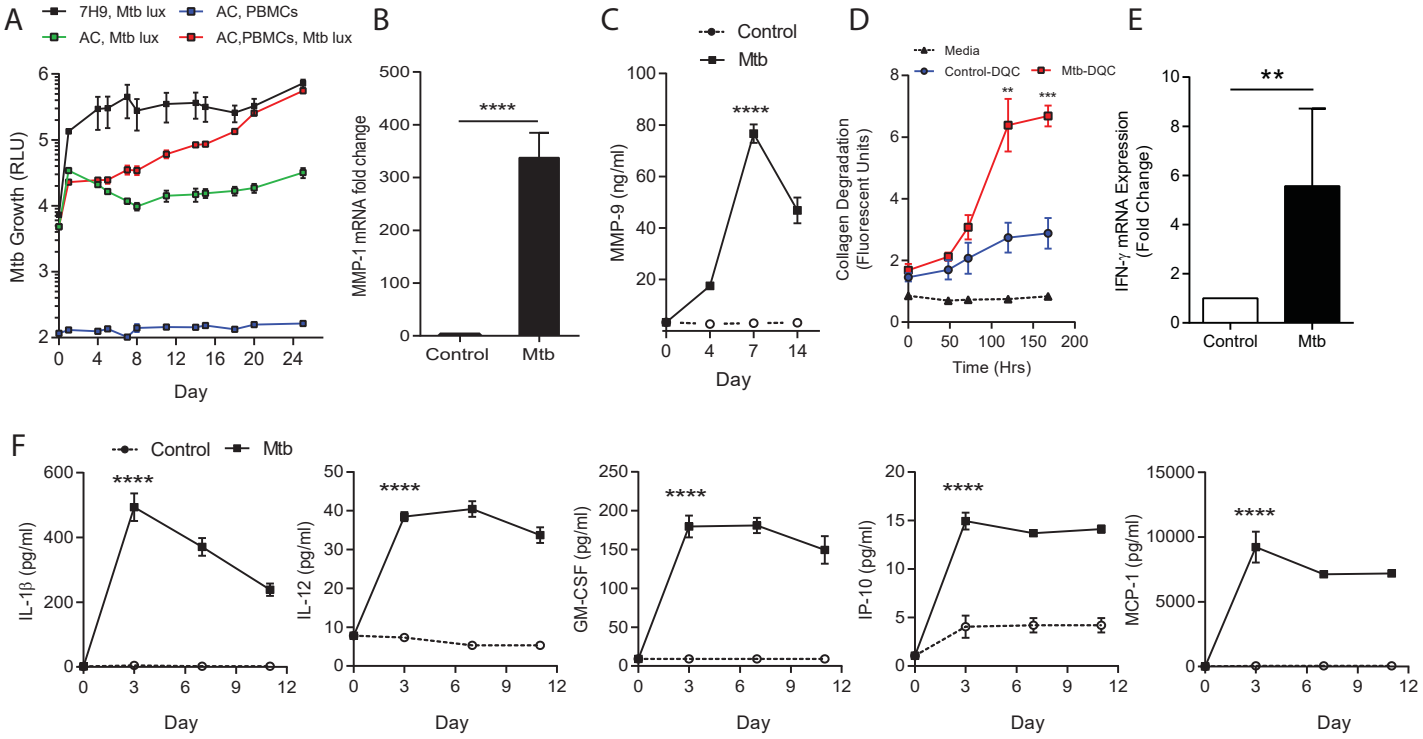

Figure 2: Mtb grows within microspheres containing PBMCs and upregulates MMP and cytokine expression. **A.** Mtb proliferates slowly in microspheres with no cells (green line), but progressively in microspheres containing PBMCs (red line), reaching similar luminescence to Middlebrook 7H9 broth culture at 24 days (black line). Blue line, uninfected microspheres. **B.** Mtb infection upregulates MMP-1 gene expression and (**C**) MMP-9 secretion in microspheres. **D.** MMP upregulation has a functional effect, causing collagen degradation. DQ Collagen breakdown is higher in Mtb-infected microspheres (red line) than uninfected (blue line). Triangles, microspheres with no PBMCs. **E.** Mtb infection increases cellular IFN-γ mRNA accumulation relative to uninfected cells at day 4 in microspheres (n=4). **F**. Secretion of cytokines by Mtb-infected microspheres (squares) is significantly higher than in microspheres containing uninfected PBMCs (circles). ****p< 0.0001 by t-test (B and E) and ANOVA (A, C, D, F).

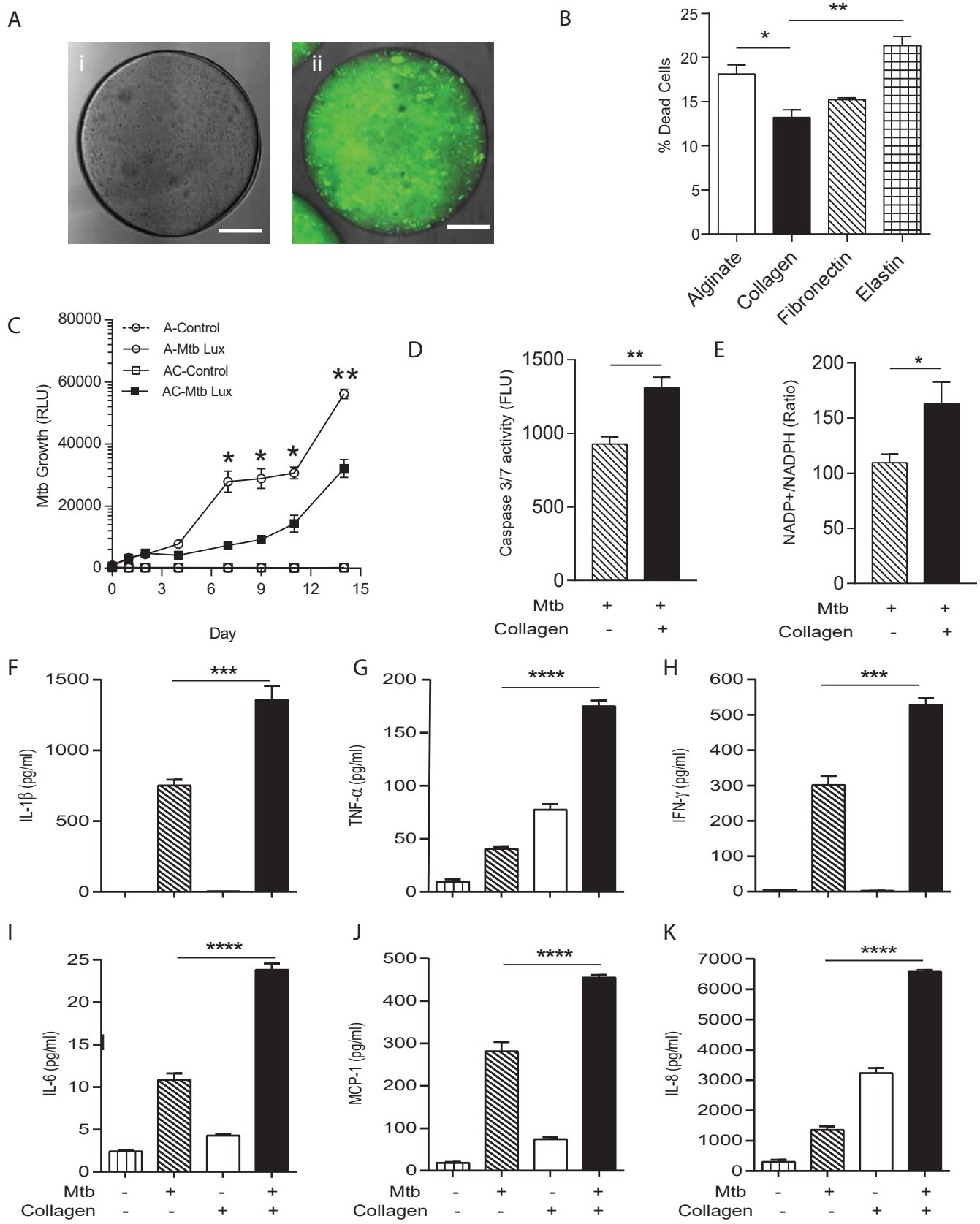

Figure 3: Incorporation of collagen into microspheres limits Mtb growth and increases host cell survival. A. Microspheres were created without collagen (i), or incorporating FITC-labelled collagen (ii) to demonstrate distribution. Immediately after bioelectrospraying, collagen is homogenous throughout the microspheres. **B.** Incorporation of Type I collagen into microspheres improves cell survival at 72h after Mtb infection, whereas elastin did not, analyzed by CytoTox-Glo assay. **C.** PBMCs control Mtb growth in microspheres containing collagen (squares) better than cells without collagen (circles). Open squares, uninfected PBMCs. **D.** The level of apoptosis and NADP+/NADPH ratio (**E**) are higher in microspheres containing collagen at day 7. Collagen incorporation caused increased secretion of IL-1β (**F**), TNF-α (**G**), IFN-γ (**H**), IL-6 (**I**), MCP-1 (**J**) and IL-8 (**K**) at day 7. Each experiment was performed a minimum of 2 times and charts represent mean values + SEM of a representative experiment performed in triplicate. * $p< 0.05$, **$p<0.01$, ***$p< 0.001$, ****$p< 0.0001$.

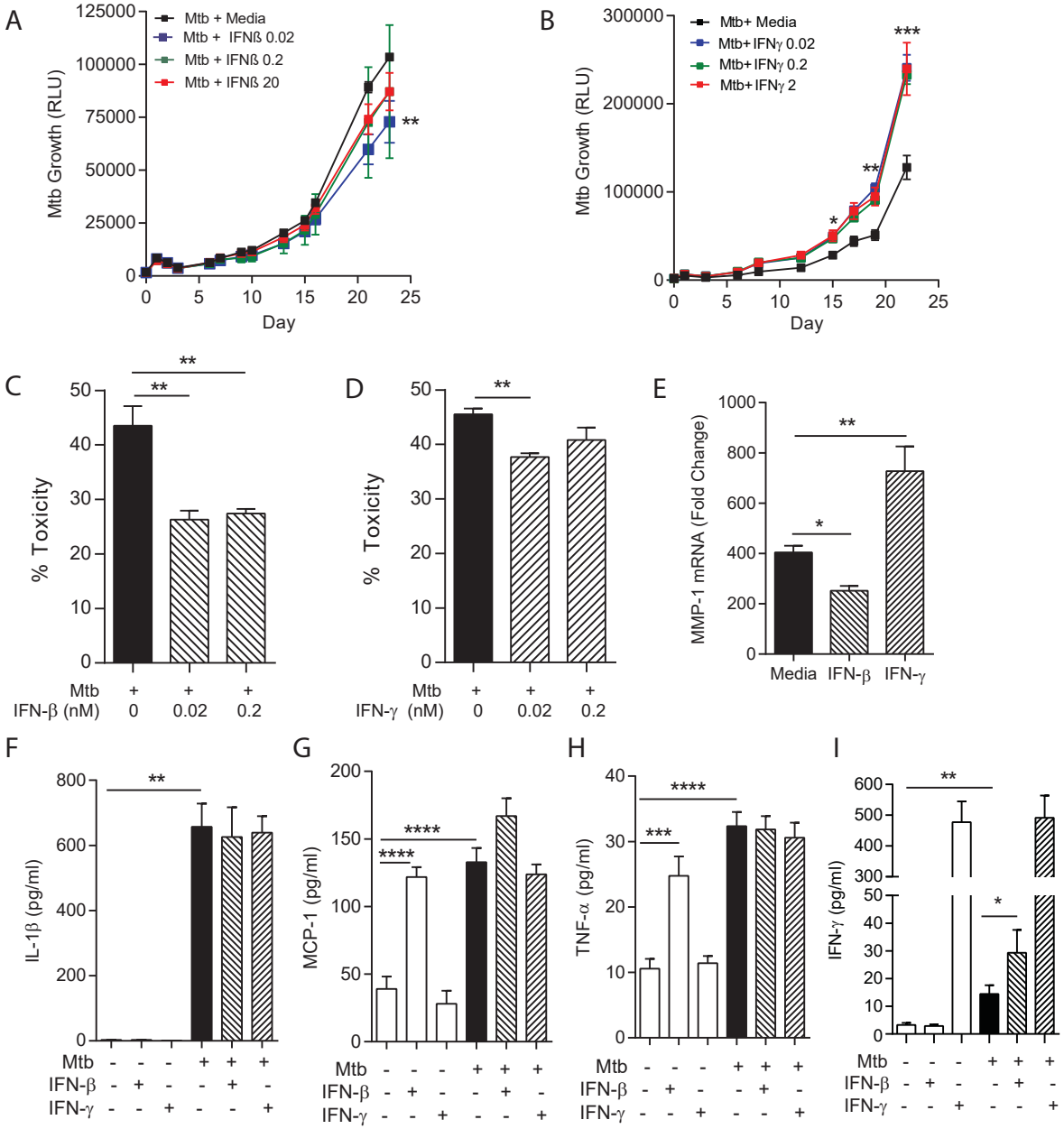

Figure 4: IFN-β and IFN-γ have divergent effects on bacterial growth within microspheres. A. Exogenous IFN-β suppresses Mtb growth after 24 days culture. Black line represents Mtb infected PBMCs. IFN-β supplementation at 0.02nM (blue), 0.2nM (green) and 2nM (red) suppresses Mtb luminescence. **B.** IFN-γ increases Mtb growth compared to infected PBMCs without additional cytokine. Exogenous IFN-γ at 0.02nM (blue), 0.2nM (green) and 2nM (red) increases Mtb luminescence above Mtb-infected PBMCs without cytokine supplementation (black line). **C, D.** Both IFN-β and IFN-γ reduce toxicity in Mtb-infected PBMCs, analyzed by CytoTox-Glo assay. **E.** IFNs divergently regulate MMP-1, with IFN-β suppressing gene expression in infected microspheres while IFN-γ increases MMP-1 expression. **F-H**. Mtb upregulates cytokine secretion but this is not modulated by IFNs. IFN-β drives TNF-α and MCP-1 as a single stimulus (E and G), but has no significant synergistic effect with Mtb. **I.** Mtb upregulates IFN-γ secretion, and this is further increased by addition of IFN-β. Mean + SEM of a representative experiment performed in triplicate is shown, and are representative of a minimum of 2 experiments done in triplicate. * $p< 0.05$, **$p<0.01$, ***$p< 0.001$ and ****$p< 0.0001$.

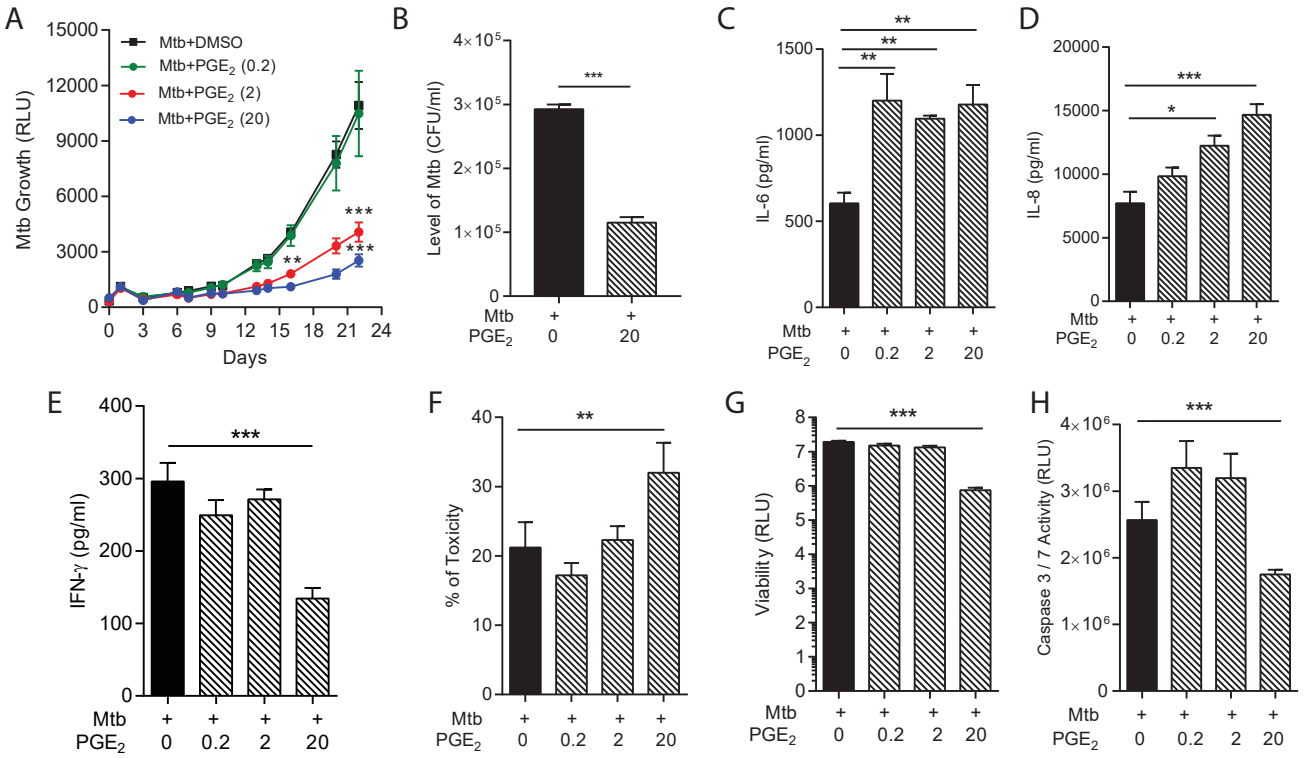

Figure 5: PGE_2 augmentation limits bacterial growth but increases pro-inflammatory cytokine secretion and cellular toxicity. A. Addition of exogenous PGE_2 suppresses Mtb growth in microspheres in a dose-dependent manner. Mtb-infected PBMCs (black line), 0.2µg/ml PGE_2 (green line), 2µg/ml PGE_2 (red line), 20µg/ml PGE_2 (blue line). **B.** Colony counts of microspheres decapsulated at day 24 and then plated on Middlebrook 7H11 agar correlate with luminescence. **C, D and E.** PGE_2 increases secretion of IL-6 and IL-8, but significantly decreases IFN-γ secretion, from Mtb-infected microspheres. **F.** Cellular toxicity is increased in PGE_2 treated microspheres at day 3, analyzed by LDH release, and (**G**) total cell viability was reduced at day 7, analyzed by CytoTox-Glo assay. **H.** PGE_2 reduces caspase 3/7 activity at day 7. *p< 0.05, **p<0.01, ***p< 0.001.

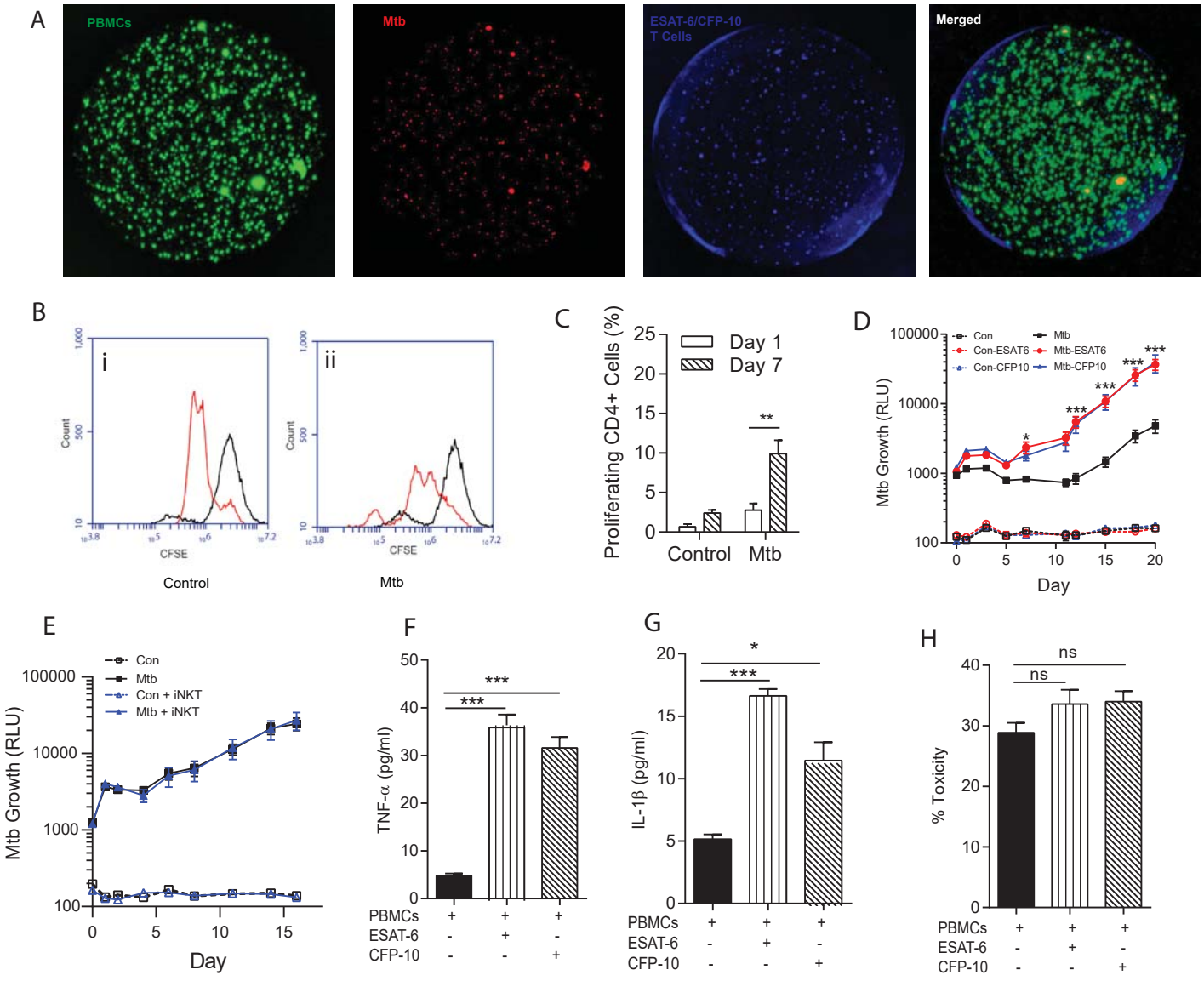

Figure 6: Immunoaugmentation with Mtb-specific T cells increases Mtb growth. A. Microspheres imaged after 4 days show early granuloma formation. (i) PBMCs labelled with CellTrace™ CFSE (green), (ii) Mtb expressing mCherry (red), (iii) autologous ESAT-6 specific T cells labelled with CellTracker Blue, (iv) Merged image shows granulomas containing Mtb, PBMCs and augmented T cells (yellow). **B.** Cellular proliferation is increased in infected microspheres with immunoaugmented autologous T cells, analysed by CFSE staining. Day 1, black line; Day 7, red line; (i) Uninfected, (ii) Mtb-infected. **C.** Quantitative analysis of the proliferative capacity of ESAT-6 augumented PBMCs at Day 1 and Day 7. The bars show percentage of proliferating CD4 cells after gating on CD3+CD4+ lymphocytes. Differences between Day 1 and 7 were assessed for three experiments by t-test. **D.** Addition of either ESAT-6 responsive T cells (red) or CFP-10 responsive T cells (blue) increases Mtb growth compared to infected PBMCs without supplemented T cells (black). Open symbols, uninfected microspheres. **E.** Supplementation with an iNKT autologous T cell line (blue triangle) did not significantly affect Mtb growth compared to infected PBMCs alone (black square). **F, G.** Secretion of TNF-α and IL-1β is increased in immunoaugmented microspheres at day 7. **H.** Immunoaugmentation did not significantly modulate cell toxicity in infected microspheres at day 3 analysed by LDH release.

A

B

Figure 1 - Supplementary figure 1: Equipment set-up within containment level 3 tuberculosis laboratory. **A.** Bioelectrosprayer housed within a double sized class I/III Microbiological Safety Cabinet. **B.** Close-up of the bioelectrosprayer cleaned after an experiment, with syringe driver on top. The external doors must be closed for microsphere generation to commence, providing the first level of containment, with the airflow of the class I MSC providing the second level of containment. The cabinet is formalin-fumigated after each experiment.

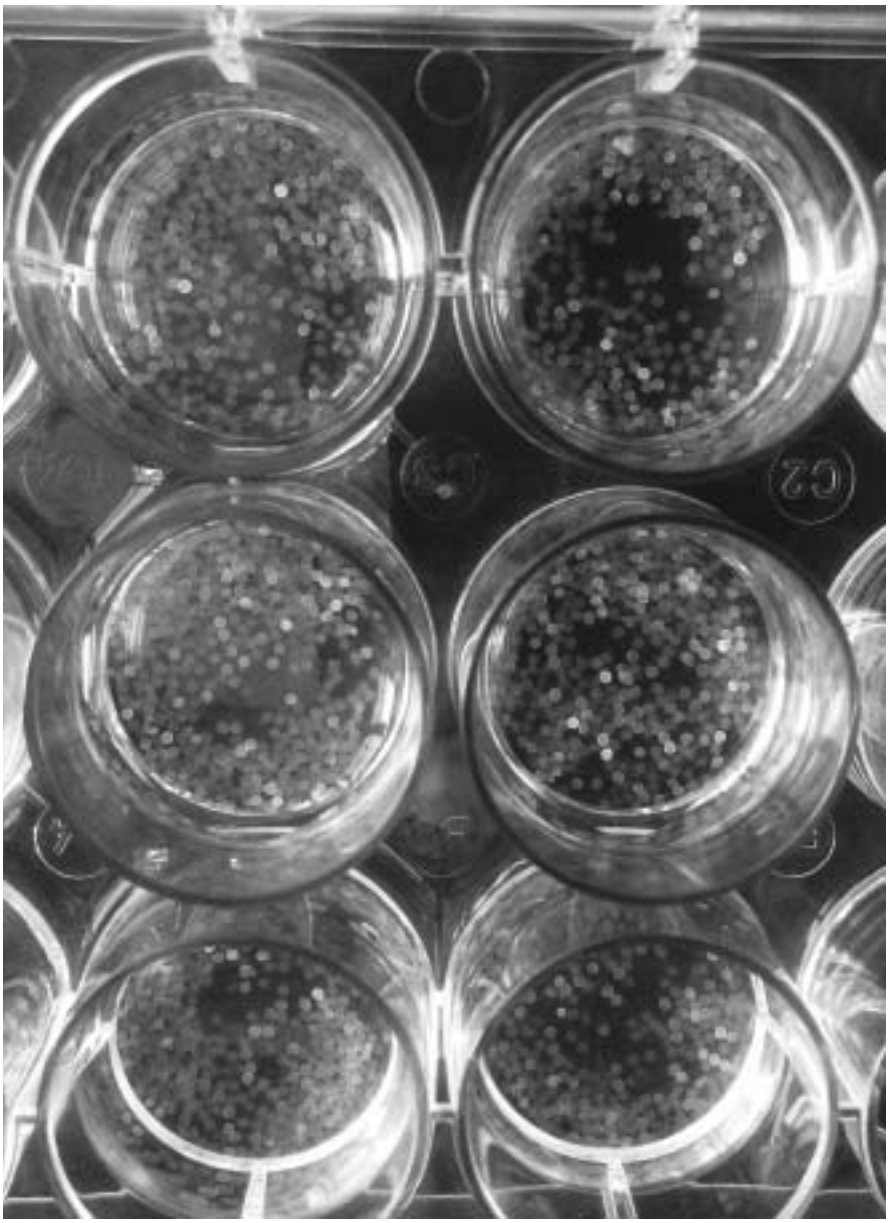

Figure 1 - Supplementary figure 2: Microspheres placed in a 12 well tissue culture plate immediately after generation demonstrating non-magnified appearance.

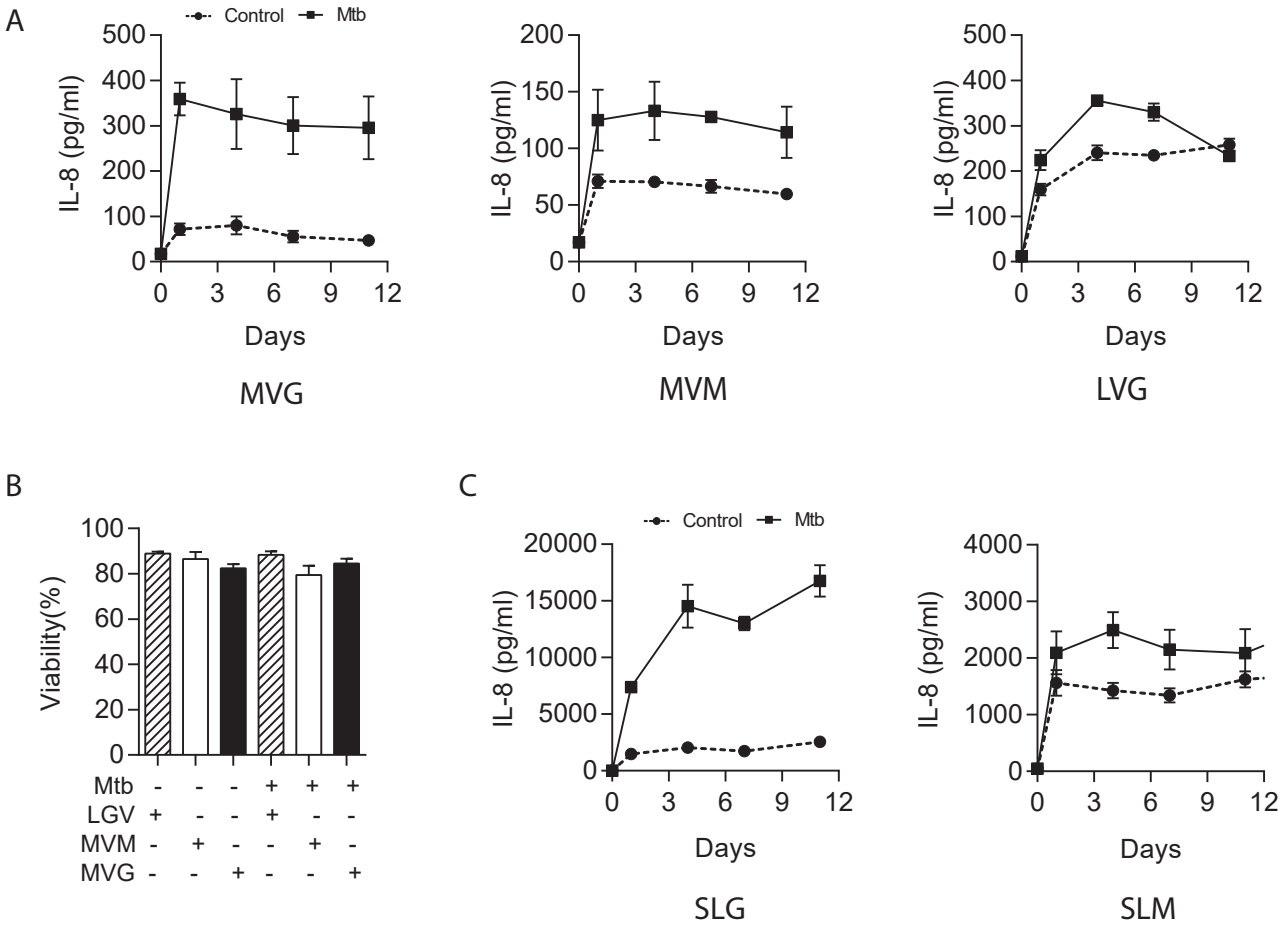

Figure 1 - Supplementary figure 3: Medium viscosity guluronate (MVG) alginate is the optimal alginate for immunological studies. **A.** IL-8 secretion from microspheres composed of different alginates measured by ELISA. MVM: medium viscosity mannuronate, LVG: low viscosity guluronate. In addition, LVG had very poor biophysical properties for biolelectrospraying. **B.** Cell viability analyzed by LDH release was not different between the different alginate types. **C.** In sterile alginate, IL-8 secretion was higher in microspheres containing SLG compared to SLM. SLG: Sterile guluronate, SLM: sterile mannuronate. Squares, filled lines: Mtb-infected microspheres, circles and broken lines: uninfected microspheres.

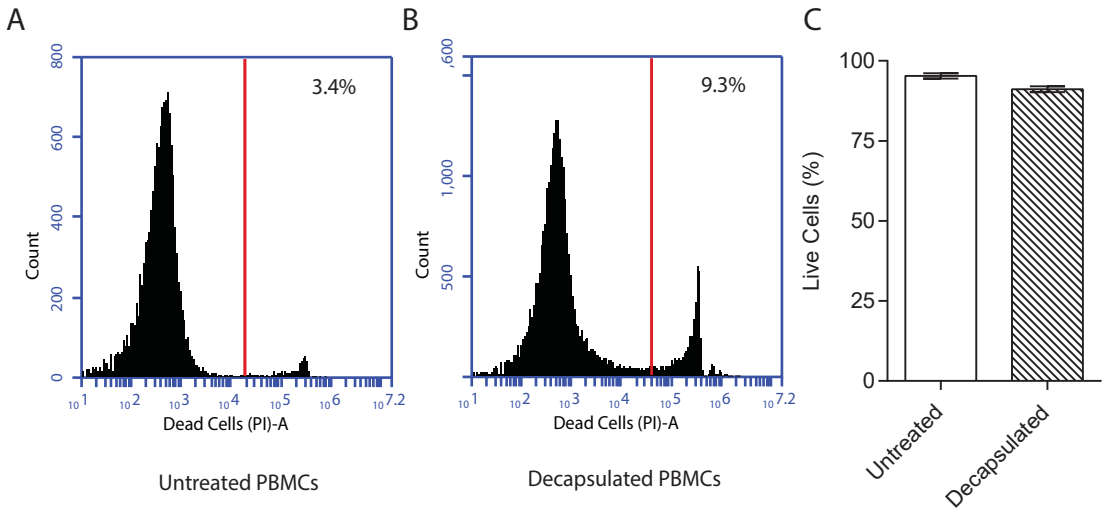

Figure 1 - Supplementary figure 4: Viability of PBMCs remains over 90% after decapsulation. PBMCs were encapsulated into alginate-collagen microspheres. After 1 hr incubation at 37°C in HBSS , they were decapsulated in solution of 55mM of sodium citrate and 5mM EDTA prepared in HBSS (pH=7.4) for 10 minutes. The cells were then washed with HBSS twice before suspension in 5 ml of RPMI and staining with propidium iodide (1mg/ml) at 1:100 dilution and analysis by flow cytometry. For comparison, viability of PBMCs kept in RPMI at 4°C during this period was used. Data is a representative of two independent experiments.

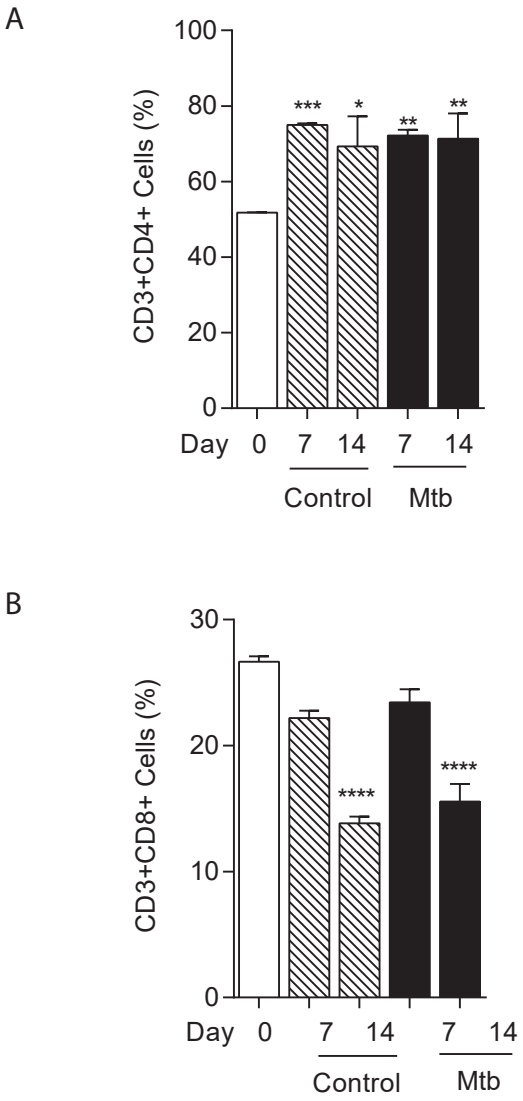

Figure 1 - Supplementary figure 5: T cell composition of microspheres. The proportion of CD4+ T cells increases between day 0 and day 7 in both uninfected and infected microspheres (A), while the proportion of CD8+ T cells falls (B). * $p< 0.05$, **$p<0.01$, ***$p< 0.001$, ****$p< 0.0001$ compared to day 0.

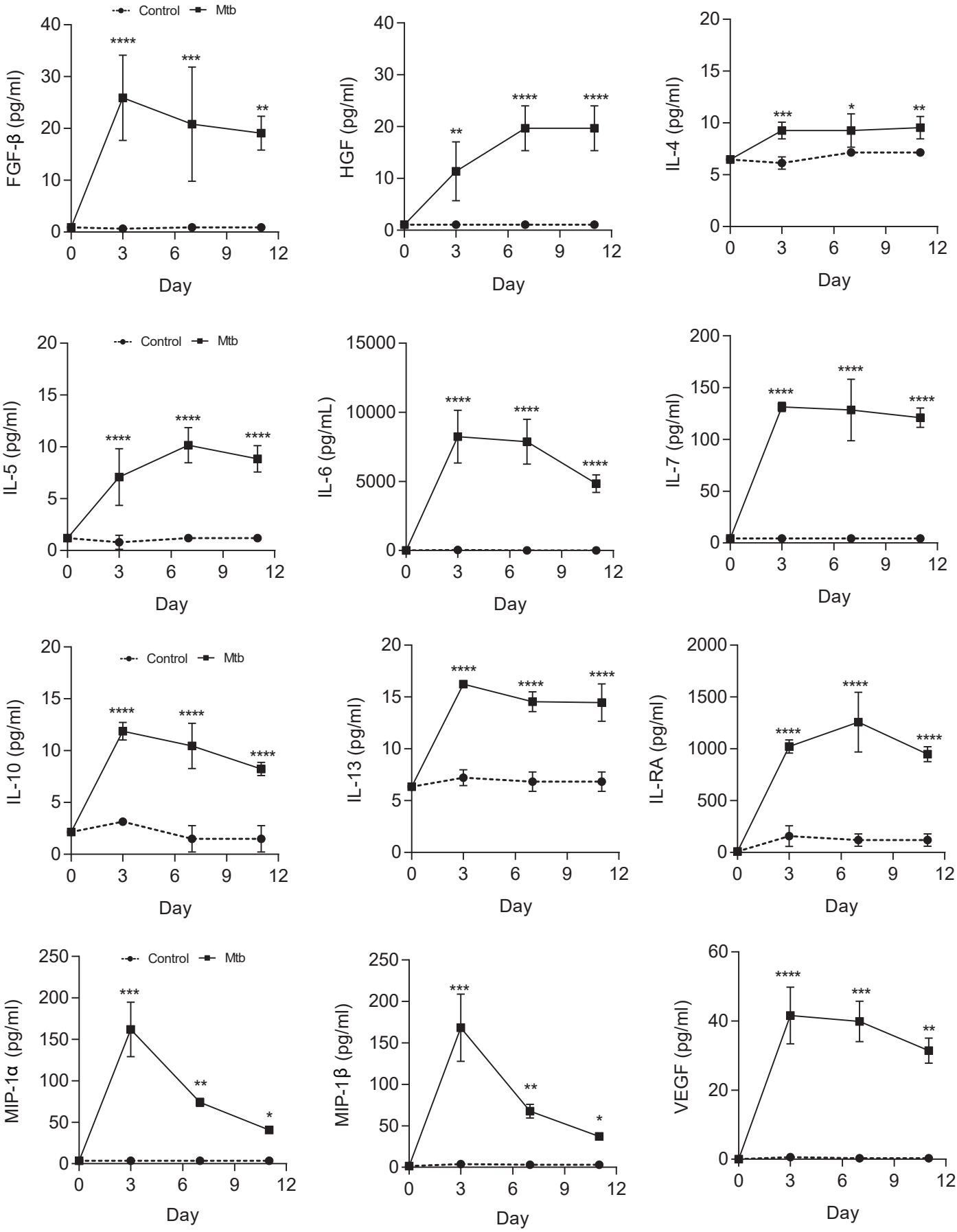

Figure 2 - Supplementary figure 1: Mtb infection upregulates secretion of multiple growth factors, cytokines and chemokines from microspheres measured by Luminex array. * $p< 0.05$, **$p<0.01$, ***$p< 0.001$, ****$p< 0.0001$ compared to uninfected microspheres at each time point.

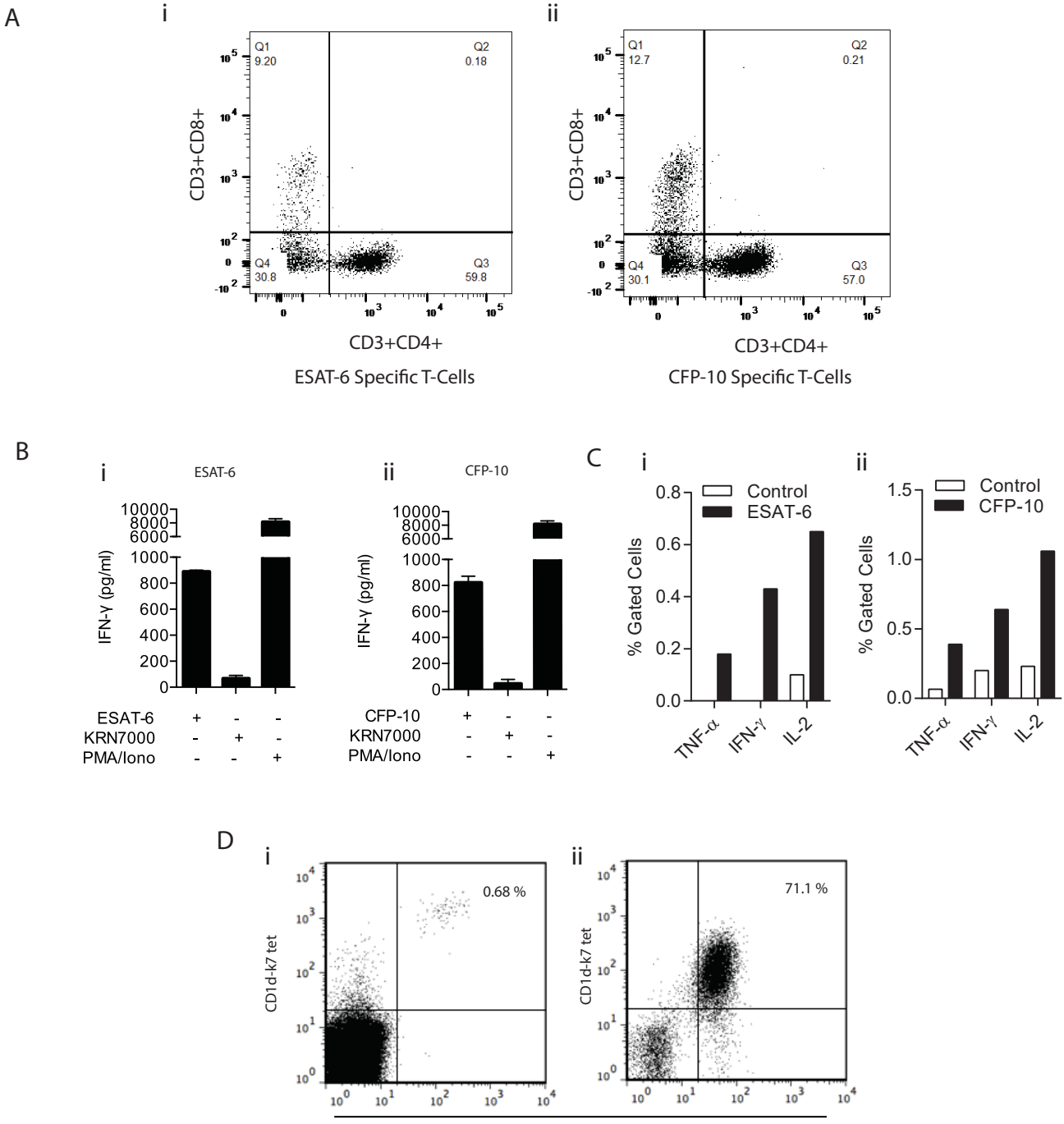

Figure 6 - Supplementary figure 1: Confirmation of specificity of *in vitro* expanded T cells. **A.** Dot plot shows percentage of T cells that are either CD4+/CD8+, CD4+/CD8-, CD4-/CD8+, CD4-/CD8- from ESAT-6 (i) and CFP-10 (ii) specific T cell lines. **B.** PBMC were cultured with ESAT-6 (i) and CFP-10 (ii) peptides and after two weeks' culture, T cell specificity was confirmed by IFN-γ release after exposure to their respective antigen. The iNKT antigen KRN7000 was used as a negative control and PMA/Ionomycin as a polyclonal T cell mitogen. Data is representative of three donors with each co-culture performed in triplicate. **C.** Percentage of ESAT-6 (i) and CFP-10 (ii) specific T cells measured by intracellular cytokine staining. Monocyte derived dendritic cells (moDCs) were pulsed with ESAT-6 or CFP-10 peptide for 12 hours prior to the addition of T cells. After 8 hours of stimulation with their corresponding antigen, each line was stained for intracellular cytokines and cells were acquired on a FACSaria. **D.** Dot plots representing *in vitro* antigen induced iNKT expansion in one donor. Live CD3+ CD1d-K7 tet+ Vα24 + iNKT cells were stained (i) *ex vivo* and (ii) 2 weeks post stimulation with KRN7000. Plots show % of iNKT cells ex vivo (0.68%) and after in vitro culture (71.1%) confirming their expansion.

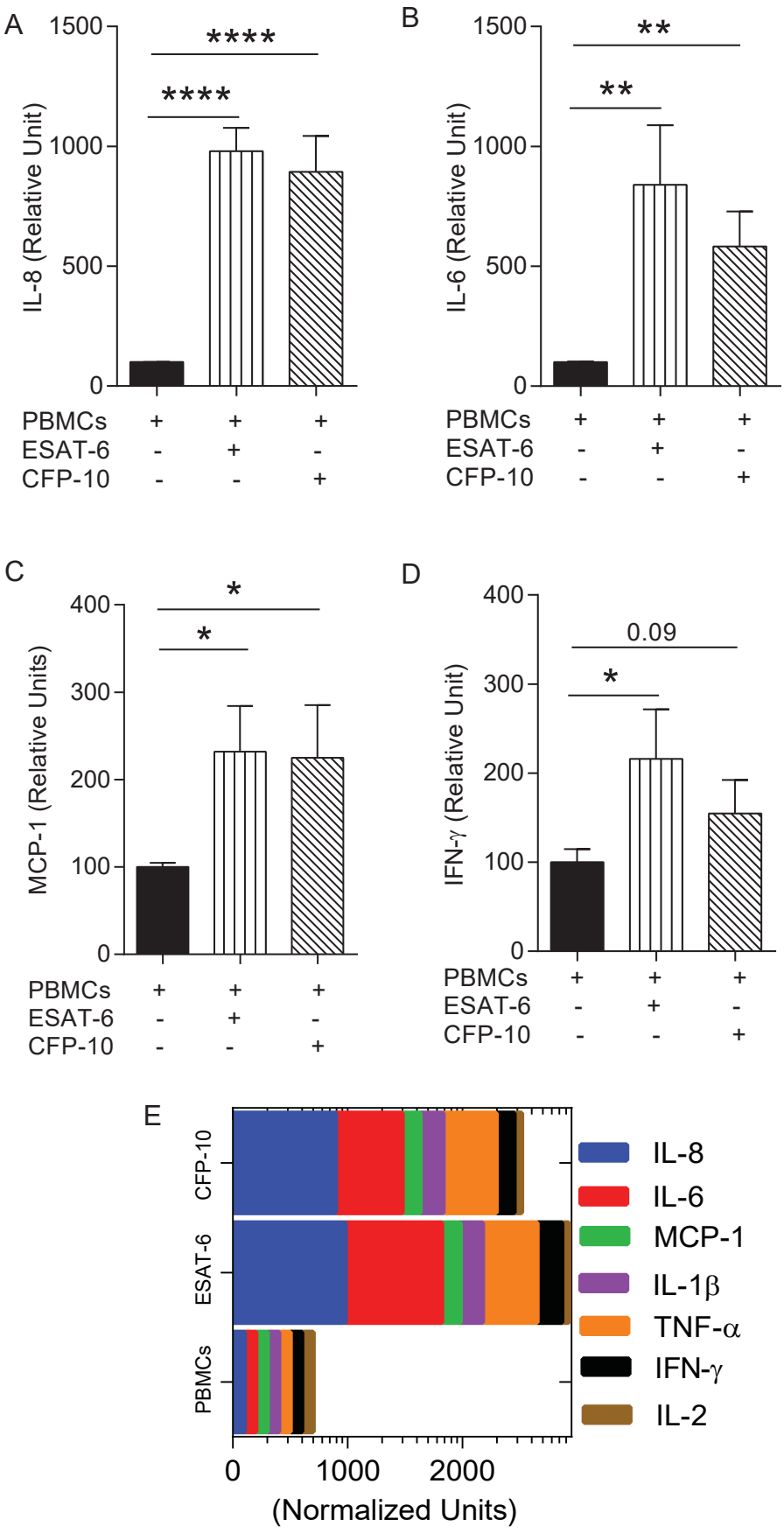

Figure 6 - Supplementary figure 2: Augmentation of PBMCs with ESAT-6/CFP-10 specific T cell lines in microspheres causes differential secretion of cytokines after Mtb infection compared to PBMCs alone. **(A-D)** Cytokine secretion in CFP-10 and ESAT-6 specific T cell supplemented microspheres was normalized to the secretion from infected PBMCs within PBMC-only microspheres and results are expressed as relative units. **(E)** Graphic representation of the cytokine profile (n=3). Data show mean ± SEM of three independent experiments done in triplicate. *p<0.05, **p<0.01, ***p<0.001, p<0.0001.